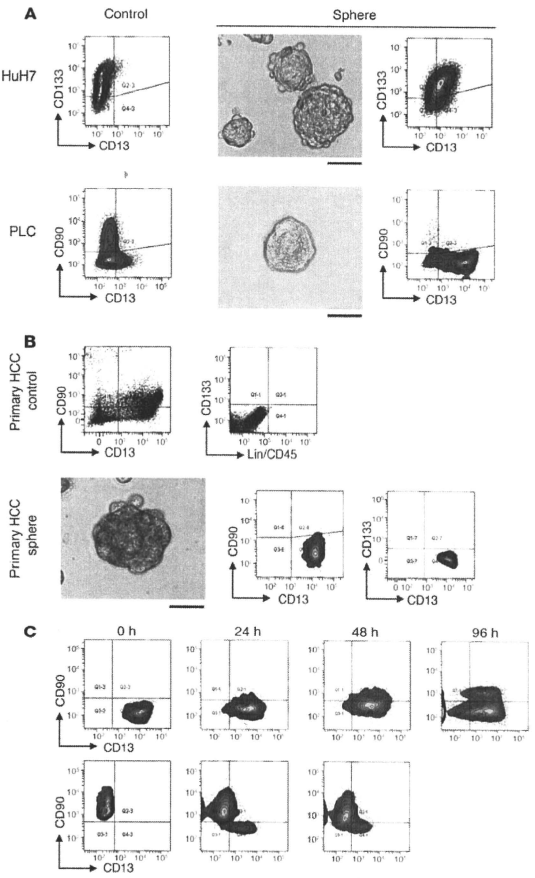

Figure 3

CD13⁺ cells exist as a core in HCC spheres and produce CD90⁺ cells. (**A**) Spheres established from HuH7 and PLC/PRF/5 cells were dissociated to single cells and the marker expressions were compared with control cells. Scale bars: 200 μm. (**B**) Expression analysis of primary human HCC cells (control) and spheres established from original human HCC cells (sphere). Scale bar: 200 μm. (**C**) The time-course expression analyses of sorted CD13⁺CD90⁻ cells (upper panels) and CD13⁻CD90⁺ cells (lower panels) from PLC/PRF/5. The cut-off lines were determined using isotype controls.

expression was increased over 20-fold by DXR or 5-FU treatment compared with control ($CD13^+CD133^+$ population in control, 2.0%; by DXR treatment, 40.3%; by 5-FU treatment, 44.3%), although expression of CD133 remained unchanged (87.1% in control vs. 88.0% after DXR treatment, 88.7% after 5-FU treatment). In PLC/PRF/5, after treatment with DXR, the $CD13^+CD90^-$ fraction was also increased and the $CD13^-CD90^+$ fraction was shifted to the CD13 positive (the $CD13^+CD90^-$ fraction of control was 15.4% and of DXR treatment was 58.2%). After treatment with 5-FU, the remaining cells were more clearly localized in the $CD13^+CD90^-$ fraction (77.8%) (Figure 4A). The chemo-resistance ability of the $CD13^+$ cells was also confirmed by cell proliferation assay in HuH7. The $CD13^+CD133^+$ fraction was highly resistant to DXR compared with the $CD13^-CD133^+$ and $CD13^-CD133^-$ fractions, indicating consistent changes in the markers following DXR treatment (Supplemental Figure 2A). Although the $CD13^-CD133^-$ fraction exhibited slow cell growth in the proliferation and cell fate study (Figure 2, B and C), this fraction showed high chemosensitivity.

Next, the effect of CD13 inhibition on cell proliferation in HuH7 was assessed. Cell proliferation was suppressed in a concentration-dependent manner after 72 hours exposure to the CD13-neutralizing antibody. At 10 and 20 μg/ml concentrations of the CD13-neutralizing antibody, cell proliferation was suppressed by approximately 80% at 24 hours and 95% at 72 hours (Figure 4B). The apoptosis assay showed that both the CD13-neutralizing antibody and CD13 inhibitor ubenimex induced apoptosis in both HuH7 and PLC/PRF/5 after 24 hours (Figure 4C). The CD13 antibody (clone WM15) has been shown to be specific to humans and to function as a neutralizing antibody (15). Reportedly, ubenimex (bestatin) specifically blocks CD13, which antagonizes the zinc-binding site of the aminopeptidase N domain (16–19). Ubenimex is used as a therapeutic agent for adult acute nonlymphatic leukemia (20).

We then hypothesized that not only the ABC transporter (21, 22) but also CD13 is involved in cell protection against exposure to anticancer agents. DXR is a well-known ABC-transporter–dependent anticancer drug. We have established a DXR-resistant HuH7 clone in which 90% of cells survive in 0.5 μg/ml of DXR, whereas about 99% of parent HuH7 cells die at that concentration (Supplemental Figure 2, B and C). Inhibition of CD13 indicated approximately 50% suppression of cell proliferation in this clone (Figure 4D), and this finding suggests that CD13 inhibition can potentially suppress cells that may have multidrug-resistance capacities and remain viable after conventional anticancer drug treatments.

CD13 is expressed preferentially in therapy-resistant HCC cells. To identify the expression of CD13 in clinical HCC, HCC samples were digested and hematopoietic Lin^-CD45^- fractions were further

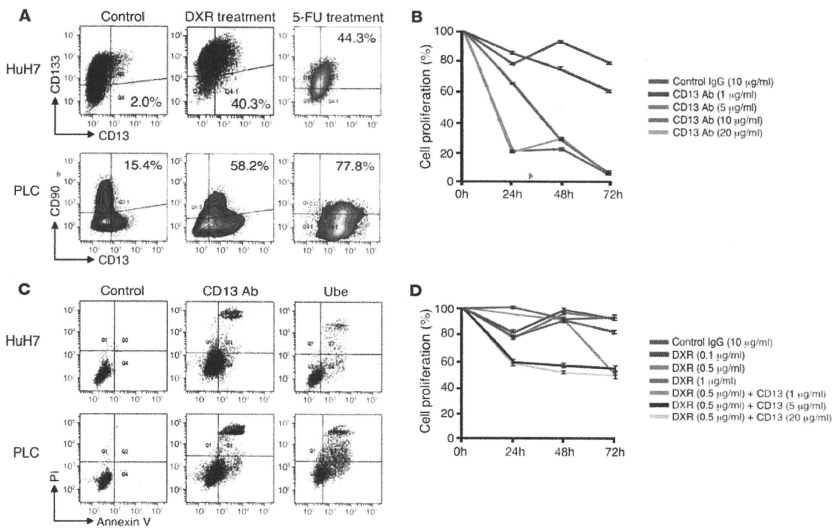

Figure 4

CD13⁺ cells resist chemotherapy, and inhibition of CD13 elicits cellular apoptosis. (**A**) The HuH7 and PLC/PRF/5 cells were treated with 0.1 μg/ml of DXR or 1 μg/ml of 5-FU for 72 hours. The changes in cell-surface markers were compared with controls. The percentages of $CD13^+CD133^+$ in HuH7 and $CD13^+CD90^-$ populations in PLC/PRF/5 are shown in figure. (**B**) Effect of CD13 inhibition on cell proliferation. HuH7 cells were treated with various concentrations of anti-human mouse IgG_1 CD13-neutralizing antibody. As a negative control, 10 μg/ml of anti-human mouse IgG_1 antibody was used. (**C**) Inhibition of CD13 induces cell apoptosis. Cells were treated with 1–20 μg/ml of CD13-neutralizing antibody or 50–500 μg/ml of ubenimex for 24 hours. Data show each case of 5 μg/ml of CD13-neutralizing antibody and 100 μg/ml of ubenimex treatment. (**D**) The effect of CD13-neutralizing antibody on DXR-R HuH7. The DXR-R clone was established with continuous treatment in 1 μg/ml of DXR and a selection of viable colonies. In 0.5 μg/ml of DXR, most control HuH7 cells die after 72 hours, whereas over 90% of DXR-R cells survive. The DXR-R HuH7 cells were cultured with 1–20 μg/ml of CD13-neutralizing antibody for 72 hours. Control, treated with 10 μg/ml of anti-human mouse IgG_1 antibody.

analyzed by multicolor flow cytometry. In all 12 clinical HCC samples, including 3 cases of non-hepatitis-derived HCC (1 case recurred after transcatheter arterial embolization [TAE]) and 9 cases of hepatitis-derived HCC (4 cases recurred after TAE), no CD133 expression was observed. In all cases, CD13 and CD90 expression was observed in the following 4 subpopulations: $CD13^+CD90^+$, $CD13^+CD90^-$, $CD13^-CD90^+$, and $CD13^-CD90^-$. In cases that recurred after TAE, the $CD13^+CD90^-$ fraction was more abundant than that in non-TAE cases (48% ± 12% in TAE cases vs. 8% ± 4% in non-TAE cases; 6-fold increase), whereas the $CD13^-CD90^+$ fraction was more abundant in non-TAE cases than in TAE cases (40% ± 18% in non-TAE cases vs. 12% ± 5% in TAE cases; 3.3-fold increase) (Figure 5A). In all 12 clinical HCC samples, the expression patterns were very similar to that of PLC/RLF/5, indicating its usefulness as an HCC model. Of course, the percentages of cells just indicate the percentage that survived after mechanical and enzymatic digestion. The majorities of HCC cells retain the cellular functions of liver cells, accumulate fat and glycogen, and produce bilirubin. Also, they are relatively bigger than other kinds of cancer cells and may be more easily damaged by mechanical and enzymatic digestion.

The expression of CD13 was confirmed in fresh frozen surgical specimens. The $CD13^+$ HCC cells typically existed along the fibrous capsule forming cellular clusters after TAE. In non-TAE cases, the $CD13^+$ HCC cells usually formed small cellular clusters inside the cancer foci (Figure 5B). CD13 was expressed on the cell surface in HCC cases. In normal liver samples, CD13 was expressed in the sinusoid with a linear staining pattern and in bile ducts with an intraductal pattern; this was different in the HCC samples. The immunohistochemical findings for the post-TAE cases support clinical experience because HCC recurrence after TAE usually occurs at the fibrous capsule and chemoresistant viable HCC cells exist mainly around the fibrous capsule.

Interestingly, some small canalicular structures near the bile ducts expressed CD13 on the cell surface, and these are suggested to be liver stem/progenitor cells, since it has been reported that normal liver stem/progenitor cells express CD13 (23). In our studies, spheres established from the normal liver were predominantly

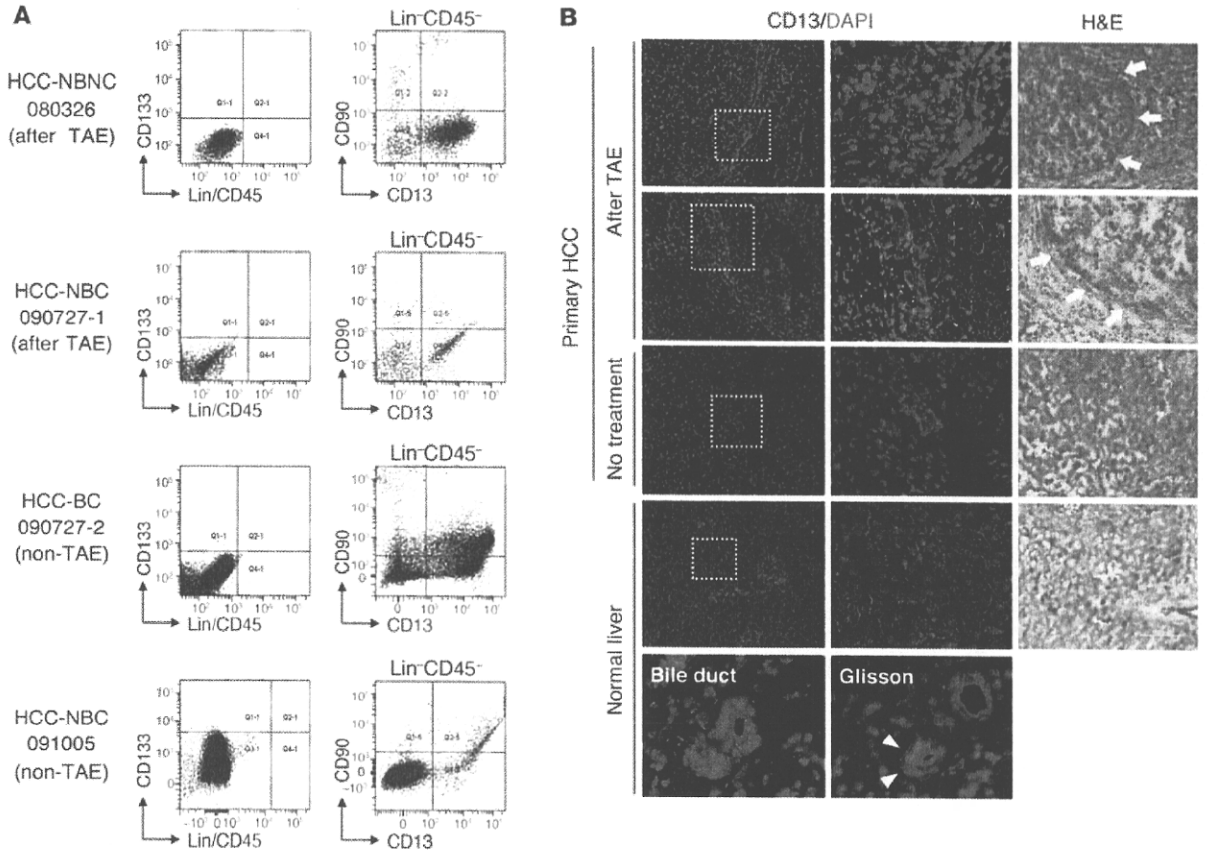

Figure 5

CD13 expression in clinical HCC samples with or without TAE. (**A**) Expression analysis of clinical HCC samples. The nonhematopoietic Lin/CD45$^-$ fraction was analyzed. The data show 2 typical TAE and non-TAE cases, nonhepatitis virus infection (NBNC; first row), nonhepatitis B but hepatitis C infection (NBC; second row), both hepatitis B and C infection (BC; third row), and another nonhepatitis B but hepatitis C infection (fourth row). The cut-off lines were determined using isotype controls. (**B**) Immunohistochemical analysis of HCC and normal liver samples stained with anti-human CD13 (red) and DAPI (blue) for the nucleus. Each middle panel shows a high magnification (×40) of the white dotted square in each left-hand column (×10). The right columns exhibit H&E stains (×10) of each adjacent frozen section. 3 typical samples from 6 HCC samples are represented. The white arrow indicates the fibrous capsule (Fc) in HCC samples, and tumor cells exist inside Fc. The upper 2 samples show HCC after TAE, and the middle samples are from no-TAE cases. In HCC samples, CD13 is expressed on the cell surface. The lower panels show immunohistochemical stains of normal liver obtained from surgical sections of colon cancer metastasis. Expression of CD13 in hepatic lobules is linear along the sinusoid. In the bile ducts, CD13 is expressed in an intraductal manner (lower left; bile duct, ×40). In some small canalicula present near the bile duct, CD13 is expressed on the cell surface (lower right; Glisson, ×40).

CD13$^+$CD90$^+$CD133$^+$, with a multidifferentiation potential in both hepatocyte and cholangiocyte lineages (Supplemental Figure 3).

To assess whether the area of the fibrous capsule contributed to the maintenance of semiquiescent CD13$^+$ cells, we stained fresh frozen tissues obtained from HCC parents with a hypoxia marker, carbonic anhydrase 9 (CA9) (24). In hematopoietic stem cells, hypoxia is well known as a hypoxic niche that plays important roles in maintaining stem cells in a dormant phase (25, 26). In the TAE samples, expression of CA9 was localized along the fibrous capsule and coexpressed CD13. In the non-TAE samples, CA9$^+$ cells formed cellular clusters in cancer foci and coexpressed CD13. In normal livers, CA9 expression was limited to the cell surface of bile ducts (Supplemental Figure 4).

CD13 inhibition elicits tumor regression. For preliminary studies, HuH7 cells were transplanted into NOD/SCID mice and treated with 5-FU to determine whether the CD13$^+$ fraction was enriched by treatment with a DNA synthesis inhibitor or not. We used 5-FU, the most common anticancer drug in HCC treatment, to simulate the clinical setting. After 3 days of intraperitoneal administration of 5-FU (30 mg/kg), most Ki67$^+$ active cells were disrupted and remained only at small foci, and tumors were replaced by a majority of CD13$^+$Ki67$^-$ cells. In the controls, CD13 expression was limited to a small fraction with cellular clustering, and most cells expressing CD13 were Ki67$^-$. Conversely, in ubenimex-treated mice (20 mg/kg, 3 days), most of the CD13$^+$ cells were disrupted and replaced with Ki67$^+$ active cells (Figure 6A).

PLC/PRF/5 was then used for further analyses. The expression of markers in this cell line is similar to that in clinical HCC, and thus, the PLC/PRF/5 cell line is potentially useful as an HCC model. In control mice, CD13 expression was limited to a small fraction and most of the cells expressed CD90. After treatment with 5-FU (30 mg/kg, 5 days of injection and 2 days of withdrawal, 2 courses),

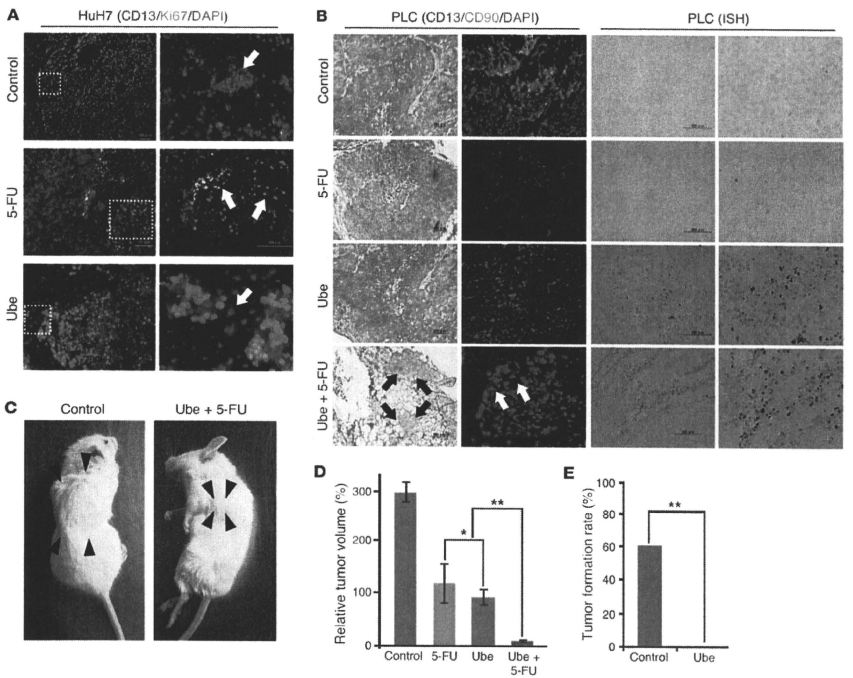

Figure 6

CD13 inhibition elicits cancer regression in vivo. (**A**) HuH7-xenografted mice were treated with 5-FU or ubenimex for 3 days. The sections were stained with anti-human CD13 (red), Ki-67 (green), and DAPI (blue). Each right-hand panel shows a high magnification (×20, control and 5-FU; ×40, Ube) of the white dot square on the left (×10, control and 5-FU; ×20, Ube). White arrows: cellular clusters express CD13 but not Ki-67 (upper panels), residual Ki-67$^+$ cancer cells (middle panels), and a residual CD13$^+$ cell (lower panels). (**B**) PLC/PRF/5-xenografted mice were treated with 5-FU, ubenimex, and ubenimex plus 5-FU for 14 days. The black arrows indicate a small amount of residual cancer. The sections were stained with H&E (×10), anti-human CD13 (red), anti-human CD90 (green), and DAPI (blue) (×20, control, 5-FU, and Ube; ×40, Ube + 5-FU). Nonspecific and fragmented expression of CD13 (white arrow). In situ hybridization for DNA fragmentation (low and high magnification). Black dot-like structures indicate labeled DNA. (**C**) Tumors of control and ubenimex–plus–5-FU–treated mice. Black arrowheads indicate the tumor margin. (**D**) The relative tumor volumes (after treatment [mm^3]/before treatment [mm^3] × 100%) of the control, 5-FU, ubenimex, and ubenimex–plus–5-FU–treated mice. Data represent mean ± SD from independent experiments. *NS; **$P < 0.01$. (**E**) The CD13$^+$ cell–enriched fractions obtained from 5-FU–treated mice were serially transplanted into secondary NOD/SCID mice. The mice were treated with ubenimex (Ube; $n = 6$) or received no treatment (control; $n = 10$) from the day after transplantation for 7 days. Tumor growth was observed for 3 weeks.

most of the CD90$^+$ cells were disrupted and tumors were replaced by a majority of CD13$^+$ cells. After ubenimex treatment (20 mg/kg every day for 14 days), not only were many CD90$^+$ cells present but CD13$^+$ cells were also identified. Interestingly, in cases in which both ubenimex and 5-FU were administered, the majority of tumor cells were disrupted. We identified atypical, nonspecific CD13 expression in these cases (Figure 6B). Taken together with the findings that CD90$^+$ cells produce CD13$^+$ cells within 24 hours and that almost all of the CD13$^+$ cells were disrupted by ubenimex plus 5-FU treatment, the CD13$^+$ cells that appeared in the ubenimex treatment groups may have been newly produced from residual CD90$^+$ cells. Costaining of Ki67 and CD13 revealed that CD13$^+$ cells were negative for the expression of Ki67 (Supplemental Figure 5).

The highly deformed nuclei observed in the ubenimex-plus-5-FU treatment specimens suggested that DNA fragments were present. The DNA fragmentation status was thus assessed by in situ hybridization with terminal deoxynucleotidyl transferase (TdT). There were a few DNA fragments in both the control and 5-FU–treated specimens, whereas there were many more in the ubenimex-treated specimens. Especially in the specimens treated

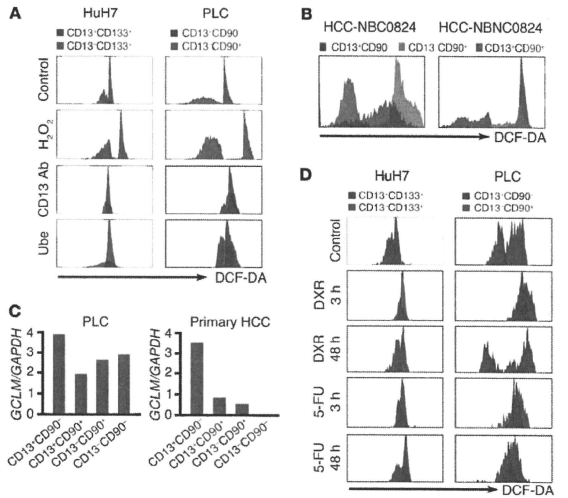

Figure 7

CD13⁺ cells contain lower levels of ROS than CD13⁻ cells. (**A**) The expression of prooxidant DCF-DA in CD13⁺CD133⁺ and CD13⁻CD133⁺ HuH7 cells and CD13⁺CD90⁻ and CD13⁻CD90⁺ PLC/PRF/5 cells. Controls, treated with 10 μg/ml of mouse anti-human IgG. As positive controls, cells were treated with 100 μM of oxidant H_2O_2 for 2 hours. Cells were treated with 5 μg/ml of CD13-neutralizing antibody and 25 μg/ml of ubenimex for 4 hours. (**B**) The expression of ROS in the CD13⁺CD90⁻, CD13⁻CD90⁺, and CD13⁺CD90⁺ fractions of 2 clinical HCC samples. (**C**) The expression of the ROS scavenger pathway gene *GCLM* in isolated CD13⁺CD90⁻, CD13⁺CD90⁺, CD13⁻CD90⁺, and CD13⁻CD90⁻ cells from PLC/PRF/5 and clinical HCC samples estimated by semiquantitative RT-PCR. (**D**) The time-course change of ROS expression in DXR or 5-FU treatment. Cells were treated with 1 μg/ml of DXR and 1 μg/ml of 5-FU continuously. After 3 hours and 48 hours of treatment, ROS levels in each population were measured.

with ubenimex plus 5-FU, there were numerous DNA fragments in residual tumor cells (Figure 6B).

After 14 days of treatment, the tumor volume was significantly decreased in the ubenimex–plus–5-FU groups compared with the control and 5-FU or ubenimex groups (Figure 6, C and D).

Next, we studied the effects of CD13 inhibition as it pertains to the self-renewing ability of cells and repopulation of tumors. The CD13⁺-enriched fraction obtained from 5-FU–treated mice was serially transplanted into secondary NOD/SCID mice. Starting the day after transplantation, the mice were treated with ubenimex (20 mg/kg) for 7 days. After 3 weeks, no tumor formation was observed in the ubenimex-treated mice (n = 0/6), whereas 60% of the untreated mice grew tumors (n = 6/10) (Figure 6E).

The CD13⁺ HCC cells contain lower levels of ROS. We focused on the ROS scavenger pathway to determine why DNA fragmentation and apoptosis were induced by CD13 inhibition. It has been reported that self-renewing dormant stem cells normally possess low levels of intracellular ROS and that deregulation of ROS levels impairs stem cell functions (27). Intracellular ROS levels were measured by prooxidants using the 2′,7′-dichlorofluorescein diacetate (DCF-DA) stain. Both in HuH7 and PLC/PRF/5, the CD13⁺ fraction contained lower concentrations of ROS than the $CD133^{strong}$ and CD90⁺ fractions. After stimulation of oxidative stress by H_2O_2, a lower concentration of ROS was clearly observed in the CD13⁺ fraction compared with the CD13⁻ fraction. Following treatment with the CD13-neutralizing antibody or ubenimex, the ROS concentration was significantly increased in CD13⁺ cells and reached the level of ROS observed in the CD13⁻ fraction (Figure 7A). In clinical HCC samples, the results were similar to those in PLC/PRF/5, as the CD13⁺CD90⁻ fraction exhibited lower ROS levels than those in the CD13⁻CD90⁺ and CD13⁺CD90⁺ fractions (Figure 7B). The CD13⁺ fraction also contained another ROS indicator, MitoSOX (a highly selective marker for mitochondrial superoxide), which was markedly lower in the PLC and clinical HCC samples and less in HuH7 (Supplemental Figure 6).

To study the correlation between CD13 and the ROS scavenger pathway, the expression of *Gclm* was assessed by RT-PCR. *Gclm* encodes the glutamate-cysteine ligase that catalyses the rate-limiting synthesis step of glutathione (GSH), which works as a critical cellular reducing agent and anti-oxidant. *Gclm* was overexpressed in the CD13⁺CD90⁻ fraction ($P < 0.001$) compared with the CD13⁺CD90⁺, CD13⁻CD90⁺, and CD13⁻CD90⁻ fractions in PLC/PRF/5 and primary HCC cells (Figure 7C).

It is well known that cell destruction after exposure to cytotoxic chemotherapy and ionizing radiation is partially due to free radicals (28, 29). Given that the present study indicates a low ROS concentration in the CD13⁺ population, we were interested to see whether chemotherapy agents actually increase ROS level of CD13⁺ population. To study this, ROS levels of CD13⁺CD133⁺ and CD13⁻CD133⁺ populations in HuH7, and CD13⁺CD90⁻ and CD13⁻CD90⁺ populations in PLC/PRF/5 were measured 3 hours and 48 hours after of DXR or 5-FU treatment. After 3 hours treatment with DXR, ROS levels were increased in both CD13⁺ and CD13⁻ populations in HuH7 and PLC/PRF/5. Interestingly, after 48-hour treatment with DXR, ROS levels of CD13⁺ populations were decreased and reached those of control levels. Especially in PLC/PRF/5, CD13⁺CD90⁻ populations showed 2 peaks of ROS levels, one of which contained further lowered ROS levels than control. With 5-FU treatment, though the power of upregulation of ROS levels was weaker than those of DXR, ROS levels of CD13⁺ fractions were actually increased to those of CD13⁻ fractions. As with the data regarding DXR treatment, after 48 hours of 5-FU treatment, CD13⁺ populations showed lower levels of ROS compared with those of the CD13⁻ population (Figure 7D). These data

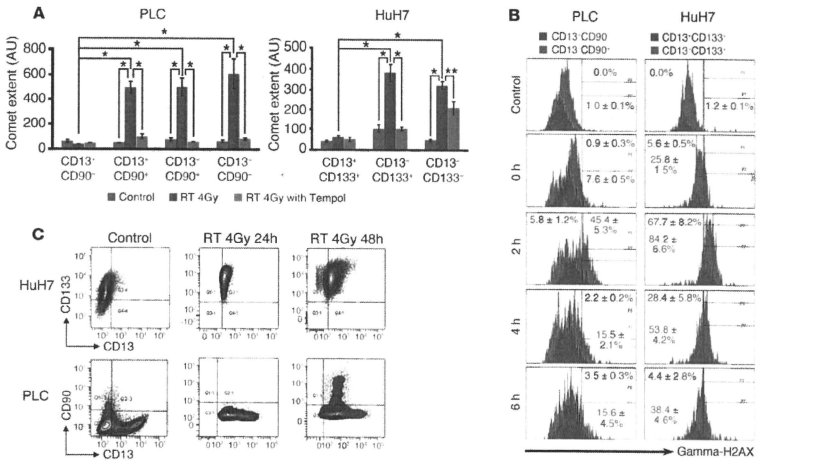

Figure 8

High levels of ROS scavenger expression parallel DNA damage in CD13$^+$ HCC cells. (**A**) Isolated cell fractions of CD13$^+$CD90$^-$, CD13$^+$CD90$^+$, CD13$^-$CD90$^+$, and CD13$^-$CD90$^-$ in PLC/PRF/5 and CD13$^+$CD133$^+$, CD13$^-$CD133$^+$, and CD13$^-$CD133$^-$ in HuH7 were irradiated with 4 Gy with or without antioxidant tempol. Data show the tail lengths in the alkaline comet assay of control (blue), 4 Gy irradiation (brown), and antioxidant tempol pretreated (green) cells. *$P < 0.01$. **NS. (**B**) HuH7 and PLC/PRF/5 cells were irradiated with 4 Gy, and time course change of gamma-H2AX expression in each population was assessed. Numbers indicate the percentage of gamma-H2AX in CD13$^+$CD90$^-$ PLC/PRF/5 and CD13$^+$CD133$^+$ HuH7 cells (red) and CD13$^-$CD90$^+$ PLC/PRF/5 and CD13$^-$CD133$^+$ HuH7 cells (blue) with ± SD. (**C**) HuH7 and PLC/PRF/5 cells were irradiated with 4 Gy, seeded in culture medium, and their expressions analyzed after 24 and 48 hours. Damaged and dead cells were eliminated with 7-AAD. The cut-off lines were determined using isotype controls.

together with the observation that CD13$^+$ cells remained after treatment with chemotherapy agents (Figure 4A), suggest that ROS levels of all of the cells are temporally upregulated when cells are treated with chemotherapy agents and that this leads to disruption of the CD13$^-$ population, whereas in the CD13$^+$ cells, ROS levels are downregulated by the ROS scavenger pathway and the cells survive. In addition, proliferative CD13$^-$ cells are easily affected by the DNA synthesis inhibition effect of chemotherapy agents.

To assess radiation-induced DNA damage with ROS, purified CD13$^+$CD90$^-$, CD13$^+$CD90$^+$, CD13$^-$CD90$^+$, and CD13$^-$CD90$^-$ PLC/PRF/5 cells were irradiated and subjected to an alkaline comet assay. Although untreated cells did not show significantly different levels of DNA damage, there were fewer DNA strand breaks in CD13$^+$CD90$^-$ cells than in the other 3 fractions ($P < 0.01$) after ionizing irradiation. The DNA damage in these 3 fractions (but not in the CD13$^+$CD90$^-$ fraction) was significantly inhibited ($P < 0.001$) by treatment with an antioxidant reagent, tempol (Figure 8A). In HuH7 cells, the CD13$^+$ fraction also exhibited lower levels of DNA damage compared with the CD13$^-$ fraction. There was no significant difference between the irradiated and tempol-treated groups for the CD13$^-$CD133$^-$ fraction (Figure 8A). These findings reveal that the enhanced ROS defenses in the CD13$^+$ fraction contribute to the reduction in DNA damage after genotoxic cancer therapy. To confirm radiation-induced DNA double-strand break status in CD13$^+$ and CD13$^-$ populations, time-course change of gamma-H2AX, a marker of double-strand breaks (30), was studied. In PLC/PRF/5, after 4 Gy of irradiation, gamma-H2AX expression in CD13$^-$CD90$^+$ population increased after 2 hours of irradiation (45.4% ± 5.3%) and then decreased within 6 hours (15.6% ± 4.5%), whereas gamma-H2AX expression in CD13$^+$CD90$^-$ population did not. In HuH7, gamma-H2AX expression increased after 2 hours in both CD13$^+$CD133$^+$ and CD13$^-$CD133$^+$ populations and decreased rapidly in the CD13$^+$CD133$^+$ population (4.4% ± 2.8%) compared with the CD13$^-$CD133$^+$ population (38.4% ± 4.6%) (Figure 8B). After 24 hours of irradiation, the residual cells were localized in the CD13$^+$ fraction in HuH7 and in the CD13$^+$CD90$^-$ fraction in PLC/PRF/5 (Figure 8C). Although there were some different manners in time-course change of gamma-H2AX in PLC/PRF/5 and HuH7, surviving cells after 24 hours of irradiation were localized in the CD13$^+$ population, suggesting the radio-resistant characteristics of the CD13$^+$ population, due to rapid recovery of DNA damage. After 48 hours of irradiation, the residual cells began to proliferate and produced CD13$^-$CD133$^+$ cells in HuH7 and CD13$^+$CD90$^+$ cells in PLC/PRF/5 (Figure 8C). These studies support the time-course studies (Figure 3C) and indicate that CD13$^+$ cells exist as a core fraction in the cellular hierarchy.

Discussion

To achieve the goal of a radical cure for cancer, recurrence and metastasis caused by residual cancer cells are barriers that need to

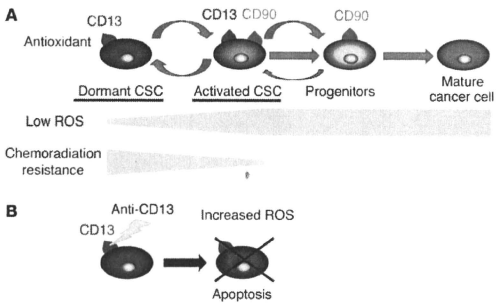

Figure 9
The CD13$^+$ CSCs of the liver generate genotoxic resistance through reduced levels of ROS (proposed schema). (**A**) Results indicate that CD13$^+$CD90$^-$ CSCs of the liver are dormant and exhibit reduced intracellular ROS levels and, because of increased antioxidants, may result in resistance to genotoxic chemo/radiation therapy. On the other hand, CD13$^-$CD90$^+$ CSCs actively proliferate and are sensitive to therapy. (**B**) Neutralization or inhibition of CD13 may result in an increase in intracellular ROS in CD13$^+$CD90$^-$ CSCs and induction of apoptosis.

be overcome. Recently, the presence of CSCs has attracted attention, and it is thought that these CSCs are intimately involved in cancer recurrence and resistance. In addition, as with leukemia (4, 5), the presence of dormant or slow-growing CSCs is beginning to be recognized in breast cancer (6). However, dormant or slow-growing CSCs have yet to be identified in most solid cancers. In the present study, we identified CD13 as a functional marker that can be used to identify potentially dormant liver CSCs resistant to treatment. Our exploration of SP cells has indicated that CD13$^+$ cancer cells are closely associated with SP cells. Cell-cycle studies indicated that CD13$^+$ cells exist in lower PY lesions. Cell-fate tracing assay with PKH26GL and immunohistochemical analysis of BrdU-retaining cells demonstrated that CD13$^+$ but not CD13$^-$ cells exhibited long dye retention and relatively slow proliferation in vitro and in vivo. This population possessed high tumorigenic potential in NOD/SCID mice and also induced chemo resistance. The results of this study are compatible with those of dormancy studies on hematopoietic stem/progenitor (3) and malignant cells (4, 5). CD13, also known as amino peptidase N, is a super family of zinc-binding metalloproteinases that play roles in cellular processes such as mitosis, invasion, cell adhesion, angiogenesis, radiation resistance, and antiapoptosis (31–34). To the best of our knowledge, there have been no reports describing the exclusive expression of CD13 in CSCs of the liver.

The immunohistochemical findings also support the view that CD13$^+$ cells play a role in relapse of liver cancer. The apparent increase in the number of CD13$^+$ cells near the fibrous capsule after TAE is consistent with the fact that clinical HCC relapse after TAE is frequent at the capsule site (7). These findings are compatible with the results of studies in mouse models that revealed that CD13$^+$ cells survived and were amplified after 5-FU treatment. In addition, the preferential accumulation of CD13$^+$ HCC cells at the capsule but not in the central region after TAE therapy suggests the attractive hypothesis that cellular components in the fibrous capsule may function as a protective niche (3).

The suppression of CD13 by the CD13-neutralizing antibody or ubenimex showed an effect even if the cancer cells were resistant to the ABC transporter–dependent agent DXR. This finding suggests that CD13$^+$ cells have some mechanism of resistance to anticancer agents in addition to their slow growth and ABC transporter (21, 35, 36) expressions. It is known that the control of ROS is indispensable for hematopoietic stem cell maintenance. Oxidative stresses inhibit cellular dormancy and self renewal of hematopoietic stem cells (37, 38). In cancer, low ROS levels and radiation resistance in CD44$^+$CD24$^-$ breast CSCs has been reported (39). However, an association between ROS and self renewal in CSCs is unknown. In the present study, we demonstrated that CD13$^+$ cells contain low levels of ROS. The CD13$^-$CD133$^+$ and CD90$^+$ cells expressed higher levels of the ROS indicators DCF-DA and MitoSOX. RT-PCR of the ROS scavenger pathway gene *GCLM* and a comet assay also indicated that CD13$^+$ cells protect themselves from oxidant stress via the ROS pathway. Continuous treatment with anticancer agents predominantly elicits high levels of ROS in the CD13$^-$ population. However, in the CD13$^+$ population, it elicits low levels of ROS, and these cells survive and are enriched for after chemotherapy. Mice treated with ubenimex exhibited high DNA fragmentation in xenografted tumors. These findings suggest that the ROS scavenger pathway and CD13 are essential to CSC protection and maintenance in the liver (Figure 9, A and B). Importantly, tumorigenicity was completely inhibited by treatment with ubenimex in secondary mice xenografted with a CD13$^+$ cell–enriched tumor fraction obtained from 5-FU–treated mice. The suppression of CD13 inhibited self renewal and the tumor-initiation ability of CD13$^+$ cells. It is thought that deregulation of ROS pathway may contribute to disruption of CSCs.

The hierarchy analysis of PLC/PRF/5 cells revealed that a small fraction of CD90$^+$ cells produce a small number of CD13$^+$ cells in vitro. This finding indicates that activated CD90$^+$ cells should also be involved in targeted cancer therapy. The CD90$^+$ cells were resistant and remained in spite of treatment with ubenimex in vivo. The residual CD90$^+$ cells cause cancer regrowth and cancer recurrence by producing tumor-initiating CD13$^+$ cells. CD13$^+$ cells have high tumorigenicity and self-renewal ability in vivo. But unfortunately, in the case of liver cancer, it is difficult to target the proliferative CD90$^+$ cells by using conventional anticancer drugs because some parts of CD90$^+$ cells also express CD13. The expression of CD13 is closely related to the multidrug-resistant SP fraction, and CD13 protects cells from apoptosis via the ROS scavenger pathway. Of course, based on CSC concepts, tumors will disappear when CSCs are disrupted completely. This is because the loss of CSCs leads to the destruction of the hierarchical structure within the tumor. However, it may be difficult to obtain complete pharmacokinetic control, especially in vivo. Actually, in this study, we could not achieve complete disappearance of CD13$^+$ cells and

could not elicit tumor regression by single agent administration of ubenimex. To overcome these problems, we established combination therapy with ubenimex plus 5-FU to efficiently elicit tumor regression. Ubenimex works to disrupt CD13$^+$ cells by its potential effect of upregulating ROS levels and its inhibition of self-renewal of CD13$^+$ cells. 5-FU inhibits proliferative cancer cells, decreases tumor size, and improves survival. It is known that cell destruction after exposure to cytotoxic chemotherapy and ionizing radiation is partially due to free radicals (29, 39), and it is reported that 5-FU induces ROS in hematopoietic stem cells and suppresses the hematopoietic stem cell niche (40). We have also confirmed that 5-FU works to increase the ROS levels of CD13$^+$ populations. By this combination therapy, tumors were drastically regressed compared with single-agent therapy. It is suggest that 5-FU and ubenimex work in a complementary or additive fashion.

Although the majority of the experiments in this study are based on cell lines, the expression, sphere, and ROS analyses support the contention that PLC/PRF/5 cells reflect clinical HCC and may hold promise for preclinical studies. This study also suggests that the future development of liver cancer therapy based on CSC concepts appears promising. We are attempting to establish human HCC-xenografted preclinical mouse models from clinical HCC samples to provide necessary confirmation of our contention using in vivo assays.

Methods

Cell culture. Human liver cancer cells, HuH7 and PLC/PRF/5, obtained from the Cell Resource Center for Biomedical Research, Institute of Development, Aging, and Cancer (Tohoku University, Sendai, Japan) were cultured in RPMI 1640 (Invitrogen) medium with 10% FBS (Equitech-Bio). Cells were cultured at 37°C in a humidified atmosphere containing 5% CO_2.

Flow cytometric analysis and cell sorting. The antibodies used in this study are listed in Supplemental Table 1. Briefly, cells were harvested with trypsin and EDTA. Doublet cells were eliminated using FSC-A/FSC-H and SSC-A/SSC-H. Dead and damaged cells were eliminated with 7-AAD (BD Biosciences – Pharmingen). Isotype controls (BD Biosciences) were used. FcR blocking was performed using an FcR-blocking reagent (Miltenyi-Biotec). FITC-conjugated anti-human CD45 (BD Biosciences – Pharmingen) and FITC-conjugated Lineage Cocktail (Lin1; BD Biosciences – Pharmingen), which contains antibodies against CD3, CD14, CD16, CD19, CD20, and CD56 and is used to detect lymphocytes, monocytes, eosinophils, and neutrophils, were used for eliminating hematopoietic cells in the clinical sample analysis. For sorting, cells were incubated with 1 μg of each antibody for 30 minutes. Control experiments involved incubation with each antibody for 30 minutes and no apparent increase in the number of dead cells detected by propidium iodide (PI) staining.

Cell-cycle assay. To characterize the SP fractions, 1×10^6 cells in 2% FCS/1 mM HEPES buffer/DMEM were preincubated at 37°C for 30 minutes. Cells were then labeled with 10 μg/ml Hoechst 33342 (Molecular Probes) in staining medium at 37°C for 70 minutes. A total of 15 μg/ml reserpine (Sigma-Aldrich) was used for the Hoechst staining procedure. For cell-cycle analysis by PY staining, cells were first stained with Hoechst 33342 at 37°C. After 50 minutes, 1 μg/ml PY was added and the cells were incubated at 37°C for 20 minutes. FACSVantage SE DiVa (BD) and FACS SORP Aria (BD) were used for analysis and cell sorting. The cell cycle was also studied with 10 μg/ml 7-AAD (BD Biosciences – Pharmingen).

Gene expression study. Total RNA was prepared using TRIZOL reagent (Invitrogen). Reverse transcription was performed with SuperScriptIII (Invitrogen). Quantitative real-time RT-PCR was performed using a LightCycler TaqMan Master kit (Roche Diagnostics). The expression of mRNA copies was normalized against *GAPDH* mRNA expression. The PCR primers used for amplification were as follows: *GCLM*, 5′-TGTGTGATGCCACCAGATTT-3′ and 5′-TTCACAATGACCGAATACCG-3′; *GAPDH*, 5′-TTGGTATCGTGGAAGGACTCA-3′ and 5′-TGTCATCATATTTG-GCAGGTTT-3′.

Cell proliferation and chemo-resistance assay. Isolated cells were seeded into 96-well culture plates at 5×10^3 cells/well for cell proliferation assays. After 72 hours, cell viability was determined by an ATP bioluminescence assay (CellTiter-Glo Luminescent Cell Viability Assay; Promega) and the luminescence signal was detected using a luminometer (ARVO MX; Perkin-Elmer) according to the manufacturer's protocol. The cells were seeded onto 96-well culture plates at 5×10^3 cells/well. After 24 hours, DXR was added to the culture medium (0.01, 0.05, and 0.1 μg/ml). After 72 hours of exposure to the chemotherapeutic agent, cell viability was determined using a method similar to that used in the cell proliferation assay.

Cell-fate tracing. Cells were labeled with 20 μM PKH26GL (Sigma-Aldrich) according to the manufacturer's protocol. Purified populations of cells were isolated and seeded onto 4-chamber polystyrene vessel tissue culture-treated glass slides (Falcon; BD Biosciences) at 5×10^3 cells/well. Cells were cultured in RPMI 1640 (Invitrogen) medium with 20% FBS (Equitech-Bio). Cell fate was studied at each 30-minute time point for 238 hours using a time-lapse fluorescence microscope (BZ-9000 Biorevo; KEYENCE). Data were analyzed using a BZ-II analyzer (KEYENCE). BrdU-retaining cells were identified with fresh frozen samples with the modification of using 5-bromo-2′-deoxyuridine Labeling & Detection Kit 1 (Roche Applied Science) and CD13 rabbit polyclonal antibody (Santa Cruz Biotechnology Inc.). As secondary antibody, anti-rabbit IgG Alexa Fluor 555 (Molecular Probes) was used.

Sphere assay. Cells were seeded on ultra-low attachment culture dishes (Corning) in serum-free medium. DMEM/F-12 serum-free medium (Invitrogen) contained 2 mM L-glutamine, 1% sodium pyruvate (Invitrogen), 1% MEM nonessential amino acids (Invitrogen), 1% insulin-transferrin-selenium-X supplement (Invitrogen), 1 μM dexamethasone (Wako), 200 μM L-ascorbic acid 2-phosphate (Sigma-Aldrich), 10 mM nicotinamide (Wako), 100 μg/ml penicillin G, and 100 U/ml streptomycin supplemented with 20 ng/ml epithelial growth factor and 10 ng/ml fibroblast growth factor-2 (PeproTech). Digestion and cell passage were performed every 3 days.

Differentiation assays from spheres. Each single sphere established from normal liver cells was seeded into a culture chamber (BD Biosciences). Spheres were cultured in sphere medium containing 10% FBS to induce the differentiation process. Three days after the spheres became attached to the bottom of the chamber and spreading cells appeared, cells were fixed and stained with anti-human CD13 mouse monoclonal antibody (clone WM15, dilution 1:50; Santa Cruz Biotechnology Inc.), FITC-anti-human albumin goat polyclonal antibody (dilution 1:500; Bethyl Laboratories), anti-human Cytokeratin 19 mouse monoclonal antibody (clone RCK108, dilution 1:50; Dako), and anti-human α-fetoprotein mouse monoclonal antibody (clone 189502, concentration 5 μg/ml; R&D Systems).

Immunohistochemistry. The 4-μm-thick sections were obtained using cryostat and fixed with 4% paraformaldehyde for 15 minutes. After 1 hour of blocking, the sections were incubated overnight at 4°C in a humidified chamber with primary antibodies. For primary antibodies, anti-human CD13 mouse monoclonal antibodies (clone WM15, dilution 1:50; Santa Cruz Biotechnology Inc.), anti-human CA9 rabbit polyclonal antibodies (dilution 1:1000; Novus Biologicals), anti-human CD90 rabbit monoclonal antibodies (dilution 1:1000; Epitomics), and anti-human Ki-67 rabbit polyclonal antibodies (dilution 1:100; Santa Cruz Biotechnology Inc.) were used. For secondary antibodies, goat anti-mouse IgG_1, Alexa Fluor 546–conjugated, and highly cross-adsorbed (Molecular Probes) as well as goat anti-rabbit IgG, Alexa Fluor 488–conjugated and highly cross-adsorbed (Molecular Probes) antibodies were used. The coverslips were mounted using ProLong Gold and SlowFade Gold Antifade Reagent (Molecular

Probes), and the slides were viewed with a fluorescence microscope (BZ-9000 Biorevo). Data were analyzed using BZ-II (Keyence). The continuous cryostat sections were also stained with modified H&E.

Tumor cell preparation. Primary liver cancer samples were obtained from Osaka University with the patients' informed consent and the approval of the Research Ethics Board of Osaka University. Tumor tissues were cut into approximately 2-mm fragments, further minced with a sterile scalpel, and washed twice with DMEM/10% FBS. They were then placed in DMEM/10% FBS with 2 mg/ml collagenase A (Roche Diagnostics) solution. The mixture was incubated at 37°C with shaking until digestion was complete. Cells were filtered through a 40-μm nylon mesh and washed twice and the cell fragments and debris were then eliminated by Ficoll (GE Healthcare) density gradient centrifugation and stained for flow cytometry.

Inhibition of CD13. A total of 5×10^3 cells were seeded into 96-well plates in 200 μl of culture medium. After 24 hours, the medium was replaced with fresh culture medium containing 1, 5, 10, and 20 μg/ml mouse monoclonal anti-human CD13 antibodies (clone WM15; GeneTex) or 25, 50, 100, 250, and 500 μg/ml ubenimex (Nippon Kayaku). Cell viability was assayed at 24, 48, and 72 hours using Cell Counting Kit-8 (Dojindo) according to the manufacturer's instructions. Absorbance was measured at 450 nm using a 680 XR microplate reader (Bio-Rad). A total of 10 ng IgG_1 mouse monoclonal antibody (GeneTex) was used as the negative control. DXR-resistant (DXR-R) HuH7 cells were established by continuous treatment with 1 μg/ml DXR and selection of resistant colonies. Cellular apoptosis was measured using PI and APC–annexin V (BD Pharmingen) with an Apoptosis Detection Kit (BioVision).

In vivo assay. The xenografted mouse model was created by injection of 1×10^6 HuH7 and PLC/PRF/5 cells into NOD/SCID mice under anesthesia. For injection, the cells were resuspended in a 1:1 mixture of medium and Matrigel (BD Biosciences). The HuH7 cell–xenografted mice were treated with 5-FU (30 mg/kg; intraperitoneal administration) or ubenimex (20 mg/kg; oral administration) for 3 days. On the following day, mice were sacrificed and tumors were enucleated for the immunohistochemical assay. In the studies of PLC/PRF/5 cell–xenografted mice, mice were treated with 5-FU (30 mg/kg, 5 days of intraperitoneal injection and 2 days of withdrawal, 2 courses; 14 days), ubenimex (20 mg/kg, 14 days of forced oral administration), or ubenimex and 5-FU (combination of 2 courses of 30 mg/kg of 5-FU and 14 days of 20 mg/kg of ubenimex). The tumor size was calculated as follows: tumor volume (mm^3) = $a \times b/2$, where a = long axis and b = short axis. The relative tumor volume was calculated as follows: relative tumor volume (%) = $a/b \times 100$, where a = tumor volume before treatment (mm^3) and b = tumor volume after 14 days of treatment. The day after 14 days of treatment, mice were sacrificed and tumors were enucleated for immunohistochemical assay. The relative tumor volume was estimated as follows: relative tumor volume (mm^3) = tumor volume on the day after 14 days of treatment (mm^3)/tumor volume just before the start of treatment (mm^3) × 100 (%). The residual tumors after 14 days of 5-FU treatment were enucleated and minced into 2-mm squares and subcutaneously transplanted into secondary NOD/SCID mice with Matrigel. The mice were treated with ubenimex (20 mg/kg) from the day after transplantation for 7 days. Tumor growth was observed for 3 weeks. We used 4 or more mice for each model to enable statistical assessment of the results. All animal studies were approved by the Animal Experiments Committee at Osaka University.

ROS assay. To study intracellular ROS levels, cells were loaded with 10 μM of DCF-DA at 37°C for 30 minutes. ROS was activated by treatment with 100 μM H_2O_2 at 37°C for 120 minutes. To study the effect of CD13 inhibition on ROS levels, cells were pretreated with 5 μg/ml of the CD13-neutralizing antibody or 25 μg/ml of ubenimex at 37°C for 4 hours and stained with DCF-DA. For mitochondria ROS detection, cells were loaded with 5 μM MitoSOX (Molecular Probes) at 37°C for 20 minutes.

DNA fragmentation assay. For the alkaline comet assay, 5,000 isolated cells were irradiated (4 Gy) on ice and suspended in 0.6% of low melting point agarose, spread over the wells of slides, and immersed in alkaline solution for 30 minutes using a kit (Trevigen). Alkaline electrophoresis was then performed. Slides were stained with silver for visualization. For the tempol experiments, cells were treated with 10 mM of tempol (Sigma-Aldrich) for 15 minutes before irradiation. For in situ hybridization detection of fragmented DNA, 10-μm–thick serial sections obtained from fresh frozen samples were hybridized with TdT using tumor TACS in situ apoptosis detection kit (Trevigen) according to the manufacturer's protocols.

To identify DNA double-strand breaks, Alexa Fluor 488 Mouse Anti-H2AX (BD Pharmingen) was used according to the manufacturer's protocols. Briefly, cells were irradiated at 4 Gy. Cells were incubated in culture medium at 37°C in a humidified atmosphere containing 5% CO_2 after irradiation for 0, 2, 4, and 6 hours. After incubation, cells were stained with cell-surface antibodies. Then cells were fixed and permeabilized using Cytofix/Cytoperm Fixation/Permeabilization Solution Kit (BD), and stained with Alexa Fluor 488 Mouse Anti-H2AX.

Statistics. We determined statistical significance by 1-tailed Student's t test. $P < 0.05$ was defined as significant.

Acknowledgments

We thank T. Shimooka for technical assistance in this study. This work was supported in part by a grant from the Core Research for Evolutional Science and Technology (CREST), a grant-in-aid for Scientific Research on Priority Areas (20012039), a grant-in-aid for Scientific Research (category S) (21229015), and a grant-in-aid for Young Scientists (category B) (21790274) from the Ministry of Education, Culture, Sports, Science, and Technology, Japan.

Received for publication February 3, 2010, and accepted in revised form June 30, 2010.

Address correspondence to: Masaki Mori, Department of Gastroenterological Surgery, Graduate School of Medicine, Osaka University, 2-2 Yamadaoka, Suita 565-0871, Japan. Phone: 81.6.6879.3251; Fax: 81.6.6879.3259; E-mail: mmori@gesurg.med.osaka-u.ac.jp.

1. Visvader JE, Lindeman GJ. Cancer stem cells in solid tumours: accumulating evidence and unresolved questions. *Nat Rev Cancer.* 2008;8(10):755–768.
2. Lapidot T, et al. A cell initiating human acute myeloid leukaemia after transplantation into SCID mice. *Nature.* 1994;367(6464):645–648.
3. Arai F, et al. Tie2/angiopoietin-1 signaling regulates hematopoietic stem cell quiescence in the bone marrow niche. *Cell.* 2004;118(2):149–161.
4. Guan Y, Gerhard B, Hogge DE. Detection, isolation, and stimulation of quiescent primitive leukemic progenitor cells from patients with acute myeloid leukemia (AML). *Blood.* 2003;101(8):3142–3149.
5. Holyoake T, Jiang X, Eaves C, Eaves A. Isolation of a highly quiescent subpopulation of primitive leukemic cells in chronic myeloid leukemia. *Blood.* 1999;94(6):2056–2064.
6. Meng S, et al. Circulating tumor cells in patients with breast cancer dormancy. *Clin Cancer Res.* 2004;10(24):8152–8162.
7. El-Serag HB, Rudolph KL. Hepatocellular carcinoma: epidemiology and molecular carcinogenesis. *Gastroenterology.* 2007;132(7):2557–2576.
8. Haraguchi N, et al. Characterization of a side population of cancer cells from human gastrointestinal system. *Stem Cells.* 2006;24(3):506–513.
9. Ma S, et al. Identification and characterization of tumorigenic liver cancer stem/progenitor cells. *Gastroenterology.* 2007;132(7):2542–2556.
10. Ding W, et al. CD133+ liver cancer stem cells from methionine adenosyl transferase 1A-deficient mice demonstrate resistance to transforming growth factor (TGF)-beta-induced apoptosis. *Hepatology.* 2009;49(4):1277–1286.
11. Zhu Z, et al. Cancer stem/progenitor cells are highly enriched in CD133(+)CD44(+) population in hepatocellular carcinoma. *Int J Cancer.* 2009;126(9):2067–2078.
12. Yang ZF, et al. Significance of CD90+ cancer stem

cells in human liver cancer. *Cancer Cell.* 2008; 13(2):153–166.
13. Yang ZF, et al. Identification of local and circulating cancer stem cells in human liver cancer. *Hepatology.* 2008;47(3):919–928.
14. Yamashita T, et al. EpCAM-positive hepatocellular carcinoma cells are tumor-initiating cells with stem/progenitor cell features. *Gastroenterology.* 2009;136(3):1012–1024.
15. Ashmun RA, Shapiro LH, Look AT. Deletion of the zinc-binding motif of CD13/aminopeptidase N molecules results in loss of epitopes that mediate binding of inhibitory antibodies. *Blood.* 1992; 79(12):3344–3349.
16. Look AT, Ashmun RA, Shapiro LH, Peiper SC. Human myeloid plasma membrane glycoprotein CD13 (gp150) is identical to aminopeptidase N. *J Clin Invest.* 1989;83(4):1299–1307.
17. Ashmun RA, Look AT. Metalloprotease activity of CD13/aminopeptidase N on the surface of human myeloid cells. *Blood.* 1990;75(2):462–469.
18. Nakamura H, Suda H, Takita T, Aoyagi T, Umezawa H. X-ray structure determination of (2S, 3R)-3-amino-2-hydroxy-4-phenylbutanoic acid, a new amino acid component of bestatin. *J Antibiot.* 1976; 29(1):102–103.
19. Mathé G. Bestatin, an aminopeptidase inhibitor with a multi-pharmacological function. *Biomed Pharmacother.* 1991;45(2–3):49–54.
20. Kobayashi T, et al. Randomized trials between behenoyl cytarabine and cytarabine in combination induction and consolidation therapy, and with or without ubenimex after maintenance/intensification therapy in adult acute myeloid leukemia. The Japan Leukemia Study Group. *J Clin Oncol.* 1996; 14(1):204–213.
21. Hadnagy A, Gaboury L, Beaulieu R, Balicki D. SP analysis may be used to identify cancer stem cell populations. *Exp Cell Res.* 2006;312(19):3701–3710.
22. Vander Borght S, et al. Expression of multidrug resistance-associated protein 1 in hepatocellular carcinoma is associated with a more aggressive tumour phenotype and may reflect a progenitor cell origin. *Liver Int.* 2008;28(10):1370–1380.
23. Kamiya A, Kakinuma S, Yamazaki Y, Nakauchi H. Enrichment and clonal culture of progenitor cells during mouse postnatal liver development in mice. *Gastroenterology.* 2009;137(3):1114–1126.
24. Kaluz S, Kaluzová M, Liao SY, Lerman M, Stanbridge EJ. Transcriptional control of the tumor- and hypoxia-marker carbonic anhydrase 9: A one transcription factor (HIF-1) show? *Biochim Biophys Acta.* 2009;1795(2):162–172.
25. Miyamoto K, et al. Foxo3a is essential for maintenance of the hematopoietic stem cell pool. *Cell Stem Cell.* 2007;1(1):101–112.
26. Moore KA, Lemischka IR. Stem cells and their niches. *Science.* 2006;311(5769):1880–1885.
27. Naka K, Muraguchi T, Hoshii T, Hirao A. Regulation of reactive oxygen species and genomic stability in hematopoietic stem cells. *Antioxid Redox Signal.* 2008;10(11):1883–1894.
28. Estrela JM, Ortega A, Obrador E. Glutathione in cancer biology and therapy. *Crit Rev Clin Lab Sci.* 2006; 43(2):143–181.
29. Riley P. Free radicals in biology: oxidative stress and the effects of ionizing radiation. *Int J Radiat Biol.* 1994; 65(1):27–33.
30. Chen HT, et al. Response to RAG-mediated VDJ cleavage by NBS1 and gamma-H2AX. *Science.* 2000; 290(5498):1962–1965.
31. Hashida H, et al. Aminopeptidase N is involved in cell motility and angiogenesis: its clinical significance in human colon cancer. *Gastroenterology.* 2002; 122(2):376–386.
32. Menrad A, Speicher D, Wacker J, Herlyn M. Biochemical and functional characterization of aminopeptidase N expressed by human melanoma cells. *Cancer Res.* 1993;53(6):1450–1455.
33. Mishima Y, et al. Leukemic cell-surface CD13/aminopeptidase N and resistance to apoptosis mediated by endothelial cells. *J Natl Cancer Inst.* 2002;94(13):1020–1028.
34. Petrovic N, et al. CD13/APN regulates endothelial invasion and filopodia formation. *Blood.* 2007; 110(1):142–150.
35. Aihara M, et al. A combined approach for purging multidrug-resistant leukemic cell lines in bone marrow using a monoclonal antibody and chemotherapy. *Blood.* 1991;77(9):2079–2084.
36. Fairchild CR, et al. Carcinogen-induced mdr overexpression is associated with xenobiotic resistance in rat preneoplastic liver nodules and hepatocellular carcinomas. *Proc Natl Acad Sci U S A.* 1987; 84(21):7701–7705.
37. Ito K, et al. Regulation of oxidative stress by ATM is required for self-renewal of haematopoietic stem cells. *Nature.* 2004;431(7011):997–1002.
38. Ito K, et al. Reactive oxygen species act through p38 MAPK to limit the lifespan of hematopoietic stem cells. *Nat Med.* 2006;12(4):446–451.
39. Diehn M, et al. Association of reactive oxygen species levels and radioresistance in cancer stem cells. *Nature.* 2009;458(7239):780–783.
40. Hosokawa K, et al. Function of oxidative stress in the regulation of hematopoietic stem cell-niche interaction. *Biochem Biophys Res Commun.* 2007; 363(3):578–583.

Defined factors induce reprogramming of gastrointestinal cancer cells

Norikatsu Miyoshi[a], Hideshi Ishii[a,b,1], Ken-ichi Nagai[a], Hiromitsu Hoshino[a], Koshi Mimori[b], Fumiaki Tanaka[b], Hiroaki Nagano[a], Mitsugu Sekimoto[a], Yuichiro Doki[a], and Masaki Mori[a,b,1]

[a]Department of Gastroenterological Surgery, Osaka University Graduate School of Medicine, Osaka 565-0871, Japan; and [b]Department of Molecular and Cellular Biology, Division of Molecular and Surgical Oncology, Medical Institute of Bioregulation, Kyushu University, Ohita 874-0838, Japan

Communicated by Takashi Sugimura, National Cancer Center, Tokyo, Japan, November 4, 2009 (received for review August 11, 2009)

Although cancer is a disease with genetic and epigenetic origins, the possible effects of reprogramming by defined factors remain to be fully understood. We studied the effects of the induction or inhibition of cancer-related genes and immature status-related genes whose alterations have been reported in gastrointestinal cancer cells. Retroviral-mediated introduction of induced pluripotent stem (iPS) cell genes was necessary for inducing the expression of immature status-related proteins, including Nanog, Ssea4, Tra-1-60, and Tra-1-80 in esophageal, stomach, colorectal, liver, pancreatic, and cholangiocellular cancer cells. Induced cells, but not parental cells, possessed the potential to express morphological patterns of ectoderm, mesoderm, and endoderm, which was supported by epigenetic studies, indicating methylation of DNA strands and the histone H3 protein at lysine 4 in promoter regions of pluripotency-associated genes such as *NANOG*. In in vitro analysis induced cells showed slow proliferation and were sensitized to differentiation-inducing treatment, and in vivo tumorigenesis was reduced in NOD/SCID mice. This study demonstrated that pluripotency was manifested in induced cells, and that the induced pluripotent cancer (iPC) cells were distinct from natural cancer cells with regard to their sensitivity to differentiation-inducing treatment. Retroviral-mediated introduction of iPC cells confers higher sensitivity to chemotherapeutic agents and differentiation-inducing treatment.

cancer stem cells | epigenetics | pluripotent stem cells | embryonic stem cells | differentiation

Cancer is thought to be a genetic and epigenetic disease with uncontrolled proliferative potential. Although the idea was proposed decades ago, the concept that some cancer cells arise from small populations, termed cancer stem cells (CSCs), with both self-renewal potential and multipotential properties sufficient to form tumors, has emerged recently (1, 2). This small population of CSCs possesses persistent self-renewal potential that can be detected by various in vitro assessments and in vivo animal experiments (2). Therefore, it has been proposed that malignant tumors are derived from CSCs with uncontrolled proliferative potential and dysregulation of their mechanisms of differentiation (2).

The origins of CSCs remain incompletely understood (1–3). One view is that CSCs are formed as a result of alterations arising in cells that have already differentiated (1); alternatively, another notion holds that their generation is a result of tumorigenesis that has occurred in immature tissue stem cells or progenitor cells (2); however, in both theories, epigenetic organization participates in tumorigenic regulation (1, 2).

With the investigation and development of ES cells from zygote to blastodermic vesicle stages, the elucidation of the molecular mechanisms that specify pluripotent differentiation has made remarkable progress (4, 5). Regarding the regulation of molecular mechanisms managing this pluripotency, it is obvious that several types of transcription factors specifically discovered in multipotential stem cells display mutual cooperation as a result of epigenetic controls (6–9).

In this study, we analyzed the effects of transcription factor genes that were previously reported in induced pluripotent stem (iPS) cells (6, 7), as well as cancer-related oncogenes and tumor suppressor genes. The repression of tumor-suppressor genes extends the lifespan of embryonic stem (ES) cells or increases the induction efficiency of iPS cells and maintains their immortalized state (10–12). The results indicated that introduction of transcription factor genes into gastrointestinal cancer cells resulted in reprogramming of cells to a pluripotent state and sensitized them to differentiation induction. Such reprogrammed cells were distinct from parental cells. It is hoped that the generation of induced pluripotent cancer (iPC) cells will eventually accomplish some goals in this field. One such goal is the inspection of previously uncharacterized cancer treatments using differentiation therapy via the induction of drug susceptibility in cancer cells. Reprogramming of cancer cells supports the notion that transduction might cause differentiation of cells to unique cell lineages. Another goal is the exploitation of drug discoveries with the aim of producing therapeutic and diagnostic reagents and using them in their clinical applications.

Results

Expression of Genes Inducing Immature Status in Gastrointestinal Cancer Cell Lines. We performed quantitative real-time reverse transcription PCR (RT-PCR) analysis on 20 gastrointestinal cancer cell lines by using immature status-related gene primers for *NANOG, OCT3/4, SOX2, KLF4,* and *LIN28* (Fig. S1*A*). From the results of RT-PCR analysis, we selected cancer cell lines such as DLD-1, HCT116, MIAPaCa-2, and PLC, which exhibited relatively low *NANOG* mRNA expression. In these cells, immature status seems to be effectively exhibited and represented as high *NANOG* expression (6–9). Especially in the colorectal cancer cell line DLD-1, all five selected genes showed relatively low expression compared to the other gastrointestinal cancer cell lines. We then studied the induction of simultaneous combinations of several factors, which include *OCT3/4, SOX2, KLF4,* and *c-MYC*, as well as oncogenes (*BCL2* and *KRAS*) and tumor suppressor genes shRNA (*TP53, P16(INK4A), PTEN, FHIT, RB1*) (Fig. S1 *B* and *C*). These factors were transfected into four cancer cell lines with ecotropic retrovirus produced in PLAT-E packaging cells. Four transcription factors *OCT3/4, SOX2, KLF4,* and *c-MYC* significantly induced up-regulation of *NANOG* mRNA.

Induction of ES-Like State Cancer Cells with Lentiviral and Retroviral Transduction. Induction of human cancer cell lines using lentiviruses and retroviruses requires high transduction efficiencies. We optimized the transduction methods for cancer cell lines (Fig. 1*A*). The four transcription factors, *OCT3/4, SOX2, KLF4,* and *c-MYC*, were transfected into cancer cell lines with ecotropic retrovirus

Author contributions: N.M., H.I., and M.M. designed research; N.M. performed research; N.M. and H.I. contributed new reagents/analytic tools; N.M., H.I., K.N., H.H., K.M., F.T., H.N., M.S., Y.D., and M.M. analyzed data; and N.M. wrote the paper.

The authors declare no conflict of interest.

[1]To whom correspondence may be addressed. E-mail: hishii@gesurg.med.osaka-u.ac.jp or mmori@gesurg.med.osaka-u.ac.jp.

This article contains supporting information online at www.pnas.org/cgi/content/full/0912407107/DCSupplemental.

www.pnas.org/cgi/doi/10.1073/pnas.0912407107

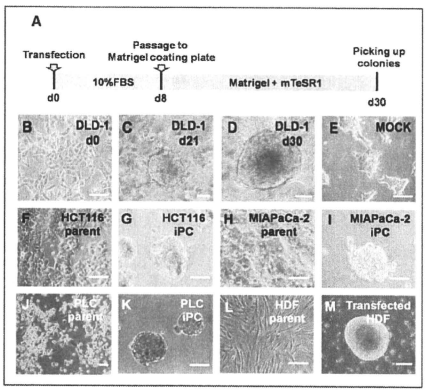

Fig. 1. Induction of human cancer cells with retroviral transduction. (*A*) We optimized the time course of the induction from human cancer cells; the schedule is summarized. (*B–E*) DLD-1 morphology was exhibited. Twenty days later, we observed distinct types of colonies with round shapes (*C* and *D*) that were different from the wild type (*B*). (*E*) Mock was transfected with pMXs Retroviral Vector as a negative control . (*F–K*) Parental and iPC cells of gastrointestinal cancer cell lines from HCT116 (*F* and *G*), MIAPaCa-2 (*H* and *I*), and PLC (*J* and *K*). (*L* and *M*) The referential morphologies are exhibited by HDF. Scale bar: 200 μm. (Original magnification, ×200)

produced in PLAT-E packaging cells. Eight days after transduction, the cells were harvested by trypsinization and plated onto Matrigel-coated plates. The next day, the Dulbecco's modified Eagle medium (DMEM) containing 10% FBS was replaced with the medium suitable for the culture of ES cells. Twenty-one days later, some colonies appeared that were morphologically different from the parental cancer cells (Fig. 1 *B* and *C*). Four weeks after transduction, we observed distinct types of colonies that were different from mock cells, transfected with pMXs retroviral vector as negative control (Fig. 1 *D* and *E*).

We examined the transfection and induction efficiencies by using combinations of *OCT3/4*, *SOX2*, *KLF4*, and *c-MYC*, and compared the results, with four cancer cell lines and human dermal fibroblasts (HDF) serving as controls (Fig. 1 *F–M*). In isolated colonies, we assessed *NANOG* promoter activity, which has been reported to be important in the acquisition of immature status (6–9), by co-transfection of *NANOG* promoter-*GFP* clone. *GFP* expression of transfectants was visualized by fluorescence microscopy (Fig. S2). From 1×10^4 cancer cells, we observed ≈10 *GFP*-expressing sphere formations. These cells in the present study were similar to iPS cells both in morphology, ES-like gene expression and epigenetic modifications as described in refs. 6–9, 13, and 14. Thus, we referred to these cells formed after transduction as iPC cells.

iPC Cells Express ES Cell Markers. Real-time RT-PCR using primers specific for retroviral transcripts confirmed efficient silencing of four retroviruses expressing *OCT3/4*, *SOX2*, *KLF4*, and *c-MYC* in iPC cells (Fig. 2*A*). RT-PCR showed that human iPC cells expressed undifferentiated ES cell-marker genes, including *NANOG*, *OCT3/4*, *SOX2*, *KLF4*, and *c-MYC*, although *NANOG* was not introduced exogenously (Fig. 2*B*). iPC cells expressed ES cell-specific surface antigens (15) including Ssea-4, tumor-related antigen (Tra)-1-60, Tra-1-81, and Tra-2-49 (Fig. 2 *C–G*) compared to the negative control (Fig. 2*H*).

In Vitro Differentiation of iPC Cells. To determine the differentiation ability of iPC cells, we used floating cultivation as embryoid bodies (EBs). Because iPC cells formed ball-shaped structures in suspension culture, we transferred these EB-like structures to EB culture conditions (EBC). These conditions were gelatin-coated plates maintained in DMEM/F12 containing 20% knockout-certified serum replacement. Culture was continued for another 7 days (Fig. 3*A*). Attached cells, named PostiPC cells, began to proliferate after 48 h. PostiPC cells were analyzed by the experiments described below and were compared to parental and iPC cells.

To determine the differentiation ability of iPC cells in vitro, we introduced iPC cells according to the methods of iPS (7). PostiPC cells showed various types of morphology, resembling those of epithelial cells, mesenchymal cells, and neuronal cells (Fig. 3 *B–E*). Immunocytochemistry detected cells that were positive for keratin 19 (Krt19) representing endoderm, vimentin (Vim) representing mesoderm and parietal endoderm, bIII-tubulin (Tubb3) representing ectoderm, and glial fibrillary acidic protein (Gfap) representing ectoderm (Fig. 3 *F–I*). RT-PCR confirmed, in addition to *VIM*, the expression of *FABP4* representing mesoderm, microtubule-associated protein 2 (*MAP2*) representing ectoderm, and paired box 6 (*PAX6*) representing ectoderm in PostiPC cells (Fig. 3*J*). The expression of *CDH1* representing endoderm and *KRT19* decreased in PostiPC cells. In particular, the gene expression of mesoderm and endoderm was increased in PostiPC cells, which was low or difficult to detect in the parental cells.

We then examined whether lineage-directed differentiation of iPC cells could be induced by methods reported for mesenchymal stem cells. We seeded iPC cells with supplements

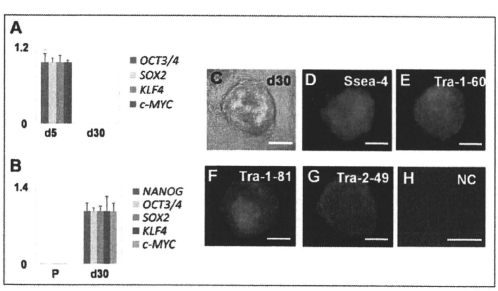

Fig. 2. iPC cells induced from DLD-1 expressing ES cell markers. (*A*) Real-time RT-PCR using primers specific for retroviral transcripts confirmed efficient silencing of four retroviruses expressing *OCT3/4*, *SOX2*, *KLF4*, and *c-MYC*. The mean value of d5 was set to 1 in each transcript. (*B*) iPC cells expressed undifferentiated ES cell-marker genes, including *NANOG*, *OCT3/4*, *SOX2*, *KLF4*, and *c-MYC*. The mean value of d30 was set to 1 in each transcript. (*C–G*) iPC cells were analyzed for several surface antigens, phase contrast (*C*), Ssea-4 (*D*), Tra-1-60 (*E*), Tra-1-81 (*F*), Tra-2-49 (*G*) and negative control (H). P, parental cells; NC, negative control. Scale bar: 200 μm. (Original magnification, ×200)

CELL BIOLOGY

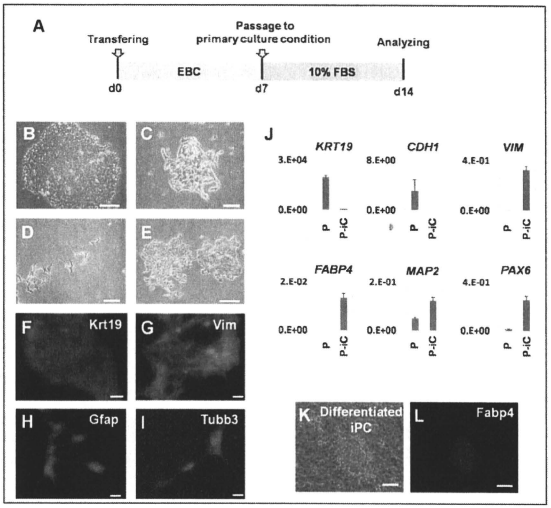

Fig. 3. Embryoid body (EB)-like formation mediated differentiation of iPC cells induced from DLD-1. (*A*) Schedule of induction from iPC cells to PostiPC cells. (*B–E*) After forming EB-like structures, iPC cells were transferred to primary culture conditions. Seven days later, attached (PostiPC) cells showed various morphologies, resembling those of epithelial cells (*B*), mesenchymal cells (*C*), neuronal cells (*D*), and mixed (*E*). (*F–I*) Immunocytochemistry confirmed the expression of Krt19 (*F*), Vim (*G*), Gfap (*H*), and Tubb3 (*I*) in these cells. (*J*) Real-time RT-PCR analysis verified the expression of differentiation markers, such as *KRT19, CDH1, VIM, FABP4, MAP2,* and *PAX6*. The expression of mRNA copies was normalized against *GAPDH* mRNA expression. (*K* and *L*) Directed differentiation of iPC cells into adipocytes showed differentiated iPC cells (*K*) that were positive for Fabp4 (*L*). P, parental cells; P-iC, PostiPC cells.

inducing adipocytes and maintained them under differentiation conditions for 2 weeks. The cells proliferated and immunocytochemistry detected cells positive for Fabp4 (Fig. 3 *K* and *L*). In contrast, immunocytochemistry on parental cells in the corresponding culture detected cells that were negative for Fabp4. These data demonstrated the possibility that iPC cells, compared to parental cells, could differentiate into three germ layers in vitro and indicated that cells acquired different properties.

Epigenetic Modification of Immature Status-Related Genes. Bisulfite genomic sequencing analyses were used to evaluate the methylation statuses of cytosine guanine dinucleotides (CpG) in the promoter regions of pluripotent-associated genes such as *NANOG*. The results revealed that the CpG dinucleotides of *NANOG* promoter were less methylated in transfected HDF (T-HDF) cells and two iPC clones, whereas the nucleotides were methylated in HDF, parental cancer cells, and PostiPC cells (Fig. 4*A*). Chromatin immunoprecipitation with trimethyl-histone H3 protein at lysine 4 (H3K4) antibody was used to analyze histone modification (Fig. 4*B*). The histone modification analyses for *NANOG* gene promoter showed that H3K4 was trimethylated in iPC, PostiPC, and T-HDF (14), whereas that of parental cancer cells and HDF was not detected. Similarly, the H3K4 trimethylation of *OCT3/4* gene promoter increased in iPC, PostiPC, and T-HDF, compared to parental cancer cells and HDF, respectively. The trimethylation of *SOX2* gene promoter was detected before and after the reprogramming of cancer cells, whereas the trimethylation of T-HDF, but not HDF, was detected. The trimethylation of *PAX6* and *MSX2* gene promoter was not detected. These findings demonstrated activation of the promoter regions of immature status-related genes in iPC cells.

Gene Expression and iPC and PostiPC Surface Markers. PostiPC cells, but not iPC cells, showed increased expression of several differentiation markers such as *FABP4, MAP2,* and *PAX6* (Fig. 3*J*), and markedly decreased expression of *NANOG, REX1, OCT3/4, SOX2, KLF4,* and *c-MYC*, which corresponded to those of parental cells (Fig. 5*A*). The expression of *P16(INK4A)* in PostiPC cells increased more than that in parental cells.

In colorectal cancer, the surface markers for CD24 and CD44 have been reported as CSC markers (16, 17). Flow cytometry showed that CD44 expression was markedly reduced in iPC cells and was increased in PostiPC cells. The CD44 expression level was relatively low in PostiPC cells compared with that of parental cells (Fig. 5*B*). CD 24 expression level was not changed apparently. The results showed the transition of the population from parental cells to PostiPC, suggesting an alteration of biological characteristics, such as sensitivity to chemicals.

Sensitivity of Anticancer Drug and Differentiation-Inducing Chemicals. The methyl thiazolyl tetrazolium (MTT) assay showed that PostiPC cells acquired sensitivity to 5-fluorodeoxyuridine (5-FU) to a greater degree than parental cells ($n = 11$, $P = 0.003$, Wilcoxon rank test; Fig. 6*A*). These data suggest the possibility that PostiPC cells, via iPC cells, could be more sensitive to therapeutic agents.

Proliferation assays for 48 h in Matrigel and the mTeSR1 medium, an ES-culture condition, showed that iPC cell growth significantly decreased compared with parental cells based on mean cell counts in four independent wells ($n = 4$, $P = 0.046$, Wilcoxon rank test; Fig. 6*B*). There was, however, no significant difference in 48-h proliferation of parental and PostiPC cells in primary culture conditions (Fig. 6*C*). An invasion assay showed no significant differences between parental and PostiPC cells (Fig. 6*D*). In a sharp contrast, the 48-h proliferation assays with the presence of retinoic acid (RA) and 1,25-dihydroxy vitamin D3 (VD3), which are known as inducers of differentiation (18, 19), resulted in a reduction in PostiPC cells compared with mock-treated parental cells ($n = 8$, $P = 0.512$ and 0.049, respectively, Wilcoxon rank test; Fig. 6 *E* and *F*). Invasion assays were performed after the 48-h treatment; the data indicated that, in the presence of RA and VD3, the invasion activity of PostiPC cells was reduced compared with parental cells ($n = 6$, $P = 0.013$ and 0.003, respectively, Wilcoxon rank test; Fig. 6 *G* and *H*).

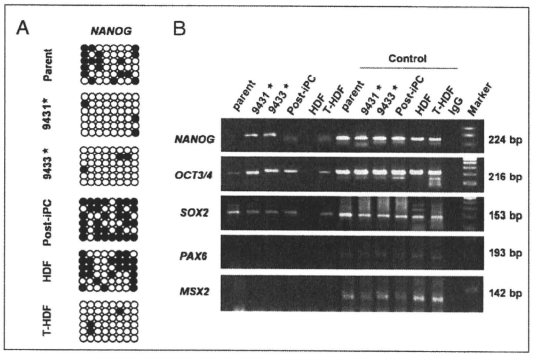

Fig. 4. Epigenetic modification of immature status-related genes evaluated with bisulfite sequencing analysis and chromatin immunoprecipitation in DLD-1. (*A*) From the analysis of epigenetic status, bisulfite genomic sequencing analyses in the promoter regions of genes inducing immature status, *NANOG*, revealed that they were not methylated appreciably in iPC cells (clones 9431 and 9433), whereas the CpG dinucleotides of the regions were methylated in parental cancer cells and PostiPC cells (open and closed circles indicate unmethylated and methylated, respectively). (*B*) Chromatin immunoprecipitation with trimethyl-K4 H3 antibody was used to analyze the histone modification status in parental, iPC, and PostiPC iCells. H3 lysine 4 was methylated in these regions for *NANOG* in iPC cells compared to that in parental and PostiPC cells. H3 lysine 4 was methylated in these regions for *OCT3/4* in iPC and PostiPC cells compared to those in parental cells (results were assessed in contrast to each input DNA). HDF and transfected HDF (T-HDF) were analyzed for comparison. As a control, respective sheared chromatin sample was used for quantitative PCR. *, clones of iPC cells.

Assessment of Tumorigenic Properties. To determine tumorigenic properties in vivo, PostiPC cells were transplanted s.c. at several densities into dorsal flanks of NOD/SCID mice. Four weeks after injection, we observed tumor formation (Fig. S3*A*). There were significant differences between PostiPC cells and parental cells ($P < 0.01$, Wilcoxon rank test; Fig. S3*B*). These data demonstrated the reduction of tumorigenesis via reprogramming process; this finding may be applied to anticancer therapy.

Discussion

The role of CSCs was noted in acute myeloid leukemia (3). The possible involvement of CSCs has since been shown in several solid tumors (20–22). In solid tumors, these results suggest that the CSC population, although it is likely a minority, is related to treatment resistance and problems of relapse or metastasis (1, 2). CSCs, through their self-renewal and drug-resistant capacities, may share properties that are conducive to persistence and proliferation, even after anticancer therapy. It is important to understand their biological characteristics, as specific markers of all CSCs have not yet been identified.

Recently, several reports have shown that tumor development is associated with genetic and epigenetic changes of the genome, and that epigenetic modifications play an important role in tumor heterogeneity (23). Several experiments, such as nuclear transplantation, ES cell fusion, and transfection with several transcription factors, have demonstrated reprogramming of terminally differentiated cells into pluripotent embryonic cells, which is linked to the development of an organism by resetting the epigenetic modifications (4–9). In previous reports, the transcription factor *NANOG* was required to maintain the pluripotency and self-renewal of ES cells (13, 14).

According to genetic and epigenetic analyses in previous reports, immature status related to promoter activation in defined genes, such as *NANOG*, plays a very important role in the establishment of a pluripotent state (6–9, 13, 14). To prepare iPC cells, we manufactured a specific tool that could detect the pluripotent

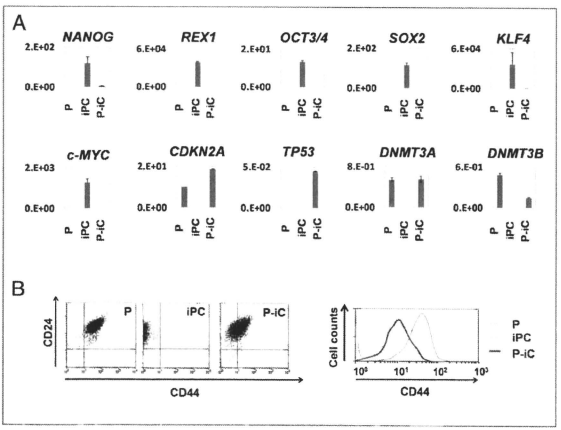

Fig. 5. Expression of immature and differentiated status-related genes in parental, iPC, and PostiPC cells induced from DLD-1. (*A*) The expression of *NANOG, REX1, OCT3/4, SOX2, KLF4, and c-MYC* markedly decreased in iPC cells. The expression of *CDKN2A, DNMT3A,* and *DNMT3B* increased in PostiPC cells compared to iPC cells. The mRNA copy expression was normalized against *GAPDH* mRNA expression. (*B*) (*Left*) Flow cytometry showed a shift of the CD24/CD44 population in parental, iPC, and PostiPC cells. (*Right*) The CD44 population in PostiPC cells decreased compared with that of parental cells. P, parental cells; P-iC, PostiPC cells.

CELL BIOLOGY

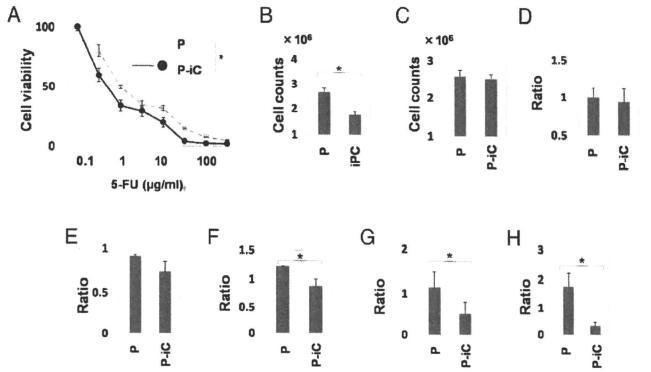

Fig. 6. In vitro methyl thiazolyl tetrazolium (MTT) analyses, proliferation and invasion assay. (*A*) The 5-FU MTT assay revealed significant differences in PostiPC and DLD-1 parental cells ($n = 11$, $P = 0.003$, Wilcoxon rank test). (*B*) Proliferation assays for ES-culture conditions showed differences in growth of iPC cells and DLD-1 parental cells ($n = 4$, $P = 0.046$, Wilcoxon rank test). (*C*) Proliferation assays in primary culture conditions showed no significant differences between DLD-1 parental and PostiPC cells. (*D*) Invasion assay showed no significant differences between DLD-1 parental and PostiPC cells (relative ratio and parental cell average). (*E* and *F*) Proliferation assays showed differences in ratio with control (with no treatment) under the differentiation-inducing treatment with vitamins A and D supplementation ($n = 8$, $P = 0.512$ and 0.049, respectively, Wilcoxon rank test). (*G* and *H*) Invasion assays showed significant differences in the ratio with control (with no treatment) cells under the differentiation-inducing treatment with vitamin A and D supplementation ($n = 6$, $P = 0.013$ and 0.003, respectively, Wilcoxon rank test). P, parental cells; P-iC, PostiPC cells. *, $P < 0.05$.

state in living cells based on the results of previous studies. We investigated *NANOG* expression in gastrointestinal cancer cell lines, corresponding to human iPS cells and teratocarcinoma NTERA-2, which had higher *NANOG* expression. The expression could not be detected in PostiPC cells with this system. A low efficiency, as shown in iPS (6–9, 13, 14), suggests a possibility that only a minority of tumor cell lines possesses specific potential to obtain the property of iPC, or more likely that multiple mechanisms are involved in full execution of reprogramming. We have to consider a possibility that sphere-forming cells might be rare among the original cancer cell populations.

In this study, the tumor-suppressor gene *P16(INK4A)*, which acts against the self-renewal of ES cells (10, 12), was repressed in iPC cells. Our analysis indicated that *P16(INK4A)* expression increased in PostiPC cells, which may relate to the notion that *P16(INK4A)* up-regulation is involved in the suppression of transformed phenotypes and their sensitization to therapeutic agents (24). The sequence study of *P16(INK4A)* promoter indicated the demethylation in PostiPC cells from DLD-1 cells, whereas the sequence of parental cells was methylated. This study suggests that the reactivation of tumor suppressor genes by reprogramming may play a role in increased chemosensitivity to 5-FU and the regression of cell proliferation and invasiveness under differentiation-inducing conditions. The *Rb/P16(INK4A)* tumor-suppressive pathway has been reported to be abrogated in several tumors (24). It is necessary to investigate the specific analysis in the pathways to assess the contribution of TSG.

Presumably, the suppression of tumors and their sensitization to induced differentiation are the result of genetic and epigenetic modifications. This result supports the possibility of new cancer therapies via reprogramming approaches even in cancer cells that should have corrupted genetic codes. In the present study, iPC cells were induced from eight cancer cells, including cancers of colorectum, esophagus, stomach, pancreas, liver and bile ducts (Fig. S4). Here, iPC was established from cancer cell lines. It is necessary to demonstrate universality in primary tumors and to more efficiently investigate the factors and population in relation to the induction of iPC cells: points to be elucidated and developed include differences of normal and tumor cells, individual responses, efficiency, and reagent delivery system. As novel therapeutic approaches, the heterogeneity of reprogrammed cancer cells remains to be investigated.

Materials and Methods

Cell Lines and Culture. Twenty cell lines derived from human gastrointestinal cancers included colorectal cancer (Caco2, DLD-1, HCT116, HT-29, KM12SM, LoVo, and SW480), esophageal cer (TE-10), gastric cancer (MKN45), pancreatic cancer (BXPC-3, MIAPaCa-2, PANC-1, and PSN-1), hepatocellular carcinoma (Hep3B, HepG2, HLE, HLF, HuH-7, and PLC), cholangiocellular carcinoma (HuCCT-1), and teratocarcinoma (NTERA-2 clone D1). NTERA-2 was provided by DS Pharma Biomedical (Osaka). These cell lines were maintained in DMEM (Nakalai Tesque, Kyoto) containing 10% FBS at 37 °C under a 5% humidified CO_2 atmosphere. HDF was purchased from Toyobo (CA106K05a; Osaka) as a normal cell control and maintained with the Fibroblast Growth Medium kit (CA116500; Toyobo). Plasmids were purchased from Addgene (Cambridge, MA), Clontech (Palo Alto, CA), Cell Biolabs (San Diego), and Open Biosystems (Huntsville, AL). The plasmids used in this study are summarized in Table S1. These transfectants were grown in DMEM supplemented with 10% FBS and puromycin (2 μg/mL), and transferred to specific culture conditions as described in the supporting information. All transfectants with retrovirus were made with the ViraDuctin retrovirus transduction kit (Cell Biolabs). Those with lentivirus were made with the Virapower packaging mix (Invitrogen, Carlsbad, CA) or Arrest-In (Open Biosystems). In brief, cancer cell lines were transfected with adequate plasmid at a concentration of 4 μg/μl by using lipofectamine (Lipofectamine 2000; Invitrogen), and incubated in glucose-free Opti-MEM (Invitrogen). All experiments were performed at 50–70% cell confluence and results were confirmed in at least three independent experiments. All-in-one-type fluorescence microscopy

(BZ-8000; Keyence, Osaka) with digital photographic capability was used to visualize cells at several magnifications. The growth rates of the cultured gastrointestinal cancer cell lines were measured by counting cells using Cell-Tac (Nihon Koden, Tokyo). The optimization of retroviral transduction of human cancer cell lines was performed as shown in supporting information. Vectors used are shown in Table S1.

RNA Preparation and RT-PCR. Total RNA was prepared by using TRIzol reagent (Invitrogen). Reverse transcription was performed with SuperScriptIII (Invitrogen). To confirm PCR amplification, 25–35 cycles of the PCR were performed by using a PCR kit (Takara, Kyoto) on a Geneamp PCR system 9600 (PE Applied Biosystems, Foster City, CA) with the following condition: 95 °C for 10 s, 60 °C for 10 s, and 72 °C for 60 s. An 8-μl aliquot of each reaction mixture was size-fractionated in a 1.5% agarose gel and visualized with ethidium bromide staining. To confirm RNA quality, PCR amplification was performed for the glyceraldehyde-3-phosphate dehydrogenase (*GAPDH*) gene using the specific primers (Tables S2 and S3). For quantitative assessment, we evaluated the gene expression by RT-PCR analysis. Quantitative real-time RT-PCR was performed by using a LightCycler TaqMan Master kit (Roche Diagnostics, Tokyo) for cDNA amplification of target specific genes. The expression of mRNA copies was normalized against *GAPDH* mRNA expression. The detailed condition for Quantitative real-time RT-PCR assessment is shown in supporting information. Primers used are shown in Tables S2 and S3.

Drugs and Antibodies. Antibodies used for immunocytology were against Nanog, Ssea-3, Ssea-4, Tra-1-60, Tra-1-81, Tra-2-49, Tubb3, Gfap, Vim (Chemicon International, Temecula, CA), and Krt19 (OriGene Technologies, Rockville, MD). Differentiation to adipocytes was induced by specific supplements (Adipogenic Supplement 390416; Invitrogen).

Bisulfite Sequencing. Genomic DNA was treated with Applied Biosystems methySEQr Bisulfite Conversion kit (Applied Biosystems) according to the manufacturer's recommendations. Treated DNA was purified with QIAquick column (Qiagen, Valencia, CA). The human *NANOG* gene promoter regions were amplified by PCR. The PCR products were subcloned with pCR2.1-TOPO. Every clone of each sample was verified by sequencing with the T3 and T7 primers. The analysis used Sequencing Analysis Software v5.2 (Applied Biosystems). Primer sequences used for PCR amplification are provided in Table S3.

Chromatin Immunoprecipitation Assay. Approximately 1×10^7 cells were cross-linked with 1% formaldehyde for 10 min at room temperature and quenched by adding glycine. The cell lysate was treated to share a chromatin-DNA complex with an enzymatic shearing kit (Active Motif, Carlsbad, CA). Immunoprecipitation used Protein G magnetic beads (Active Motif)-linked anti-trimethyl lysine 4 histone H3 antibody (Nippongene, Toyama, Japan), or a negative control IgG kit (Active Motif). Eluates were used as templates for quantitative PCR. Each sheared chromatin sample was used for quantitative PCR as a control. Primer sequences used for PCR amplification are provided in Table S3.

Flow Cytometry. Flow cytometry was performed on trypsin-dissociated parental cells, iPC, and PostiPC cells by using antibodies for CD24 (BD Biosciences, Sparks, MD) and CD44 (BD Biosciences). 7-AAD (eBioscience, San Diego, CA) preincubation was used to exclude dead cells. To assess the expression of the reprogrammed cells, iPC cells were assessed in the isolated colonies after the transfection of *NANOG* promoter-*GFP* clone. Cells were analyzed by using a FACScan flow cytometer equipped with CellQuest software (FACS caliber; BD Biosciences).

RA and VD3 Treatment. RA and VD3 were purchased from Sigma–Aldrich (St. Louis). RA was dissolved in 99% ethanol as a 100 μM stock solution. The cells were allowed to settle for 48 h in DMEM supplemented with 100 nM RA. VD3 was dissolved in 99% ethanol as a 10 M stock solution. The cells were allowed to settle for 48 h in DMEM supplemented with 10 nM VD3. To assess the proliferation in the presence of RA and VD3, the cells were grown in these media for another 48 h. Cell viability was determined with the Cell Counting kit incorporating WST-8 (Dojindo Lab., Tokyo). WST-8 (10 μL) was added to 100 μL of the medium containing each supplement above, and the absorbance was read at 450 nm by using a microplate reader (Model 680XR; Bio-Rad Laboratories, Hercules). All experiments were performed at 30–80% cell confluence, and the results were confirmed in at least three independent experiments.

Chemosensitivity Assessment. To assess the sensitivity to 5-FU in vitro, cells at different concentrations were evaluated with an MTT assay. 5-FU was purchased from Kyowa Hakkou (Tokyo). The cells were allowed to settle for 96 h in DMEM supplemented with several concentrations of 5-FU, and viability was assessed.

Invasion Assays. Cell invasion was assessed with a CytoSelect Cell Invasion Assay according to the manufacturer's protocol (Cell Biolabs). Cells (1.0×10^5) in DMEM were placed on 8.0-m-pore size membrane inserts in 96-well plates, and DMEM with 10% FBS was placed in the bottom of the wells. After 24 h, cells that did not invade were removed from the top side of the membrane chamber, and the cells from the underside of the membrane were completely dislodged by tilting the membrane chamber in Cell Detachment Solution (Cell Biolabs). Lysis Buffer/CyQuannt GR dye solution (Cell Biolabs) was added to each well, and the fluorescence of the mixture was read with a fluorescence plate reader at 480 nm/520 nm.

In Vivo Analysis. The tumorigenic properties were evaluated on trypsin-dissociated cells with parental and PostiPC cells. We transplanted them suspended in DMEM/Matrigel (BD Biosciences) s.c. into the dorsal flanks of NOD/SCID mice (CREA, Tokyo) in several concentrations. Tumors were dissected and measured 4 weeks after injection.

Statistical Analysis. For continuous variables, the results are expressed as means ± SEs of the mean. The relationships among gene expressions or cell counts were analyzed with χ^2 and Wilcoxon rank tests. All tests were analyzed with JMP software (SAS Institute, Cary, NC). Differences with P values <0.05 were considered statistically significant.

1. Reya T, Morrison SJ, Clarke MF, Weissman IL (2001) Stem cells, cancer, and cancer stem cells. *Nature* 414:105–111.
2. Pardal R, Clarke MF, Morrison SJ (2003) Applying the principles of stem-cell biology to cancer. *Nat Rev Cancer* 3:895–902.
3. Bonnet D, Dick JE (1997) Human acute myeloid leukemia is organized as a hierarchy that originates from a primitive hematopoietic cell. *Nat Med* 3:730–737.
4. Thomson JA, et al. (1998) Embryonic stem cell lines derived from human blastocysts. *Science* 282:1145–1147.
5. Hochedlinger K, Jaenisch R (2006) Nuclear reprogramming and pluripotency. *Nature* 441:1061–1067.
6. Takahashi K, Yamanaka S (2006) Induction of pluripotent stem cells from mouse embryonic and adult fibroblast cultures by defined factors. *Cell* 126:663–676.
7. Takahashi K, et al. (2007) Induction of pluripotent stem cells from adult human fibroblasts by defined factors. *Cell* 131:861–872.
8. Yu J, et al. (2007) Induced pluripotent stem cell lines derived from human somatic cells. *Science* 318:1917–1920.
9. Yu J, et al. (2009) Human induced pluripotent stem cells free of vector and transgene sequences. *Science* 324:797–801.
10. Dabelsteen S, et al. (2009) Epithelial cells derived from human embryonic stem cells display p16INK4A senescence, hypermotility, and differentiation properties shared by many P63+ somatic cell types. *Stem Cells* 27:1388–1399.
11. Hong H, et al. (2009) Suppression of induced pluripotent stem cell generation by the p53-p21 pathway. *Nature* 460:1132–1135.
12. Li H, et al. (2009) The Ink4/Arf locus is a barrier for iPS cell reprogramming. *Nature* 460:1136–1139.
13. Loh YH, et al. (2006) The Oct4 and Nanog transcription network regulates pluripotency in mouse embryonic stem cells. *Nat Genet* 38:431–440.
14. Wu Q, et al. (2006) Sall4 interacts with Nanog and co-occupies Nanog genomic sites in embryonic stem cells. *J Biol Chem* 281:24090–24094.
15. Adewumi O, et al.,International Stem Cell Initiative (2007) Characterization of human embryonic stem cell lines by the International Stem Cell Initiative. *Nat Biotechnol* 25:803–816.
16. Vermeulen L, et al. (2008) Single-cell cloning of colon cancer stem cells reveals a multi-lineage differentiation capacity. *Proc Natl Acad Sci USA* 105:13427–13432.
17. Du L, et al. (2008) CD44 is of functional importance for colorectal cancer stem cells. *Clin Cancer Res* 14:6751–6760.
18. Huang ME, et al. (1988) Use of all-trans retinoic acid in the treatment of acute promyelocytic leukemia. *Blood* 72:567–572.
19. zur Nieden NI, Kempka G, Ahr HJ (2003) In vitro differentiation of embryonic stem cells into mineralized osteoblasts. *Differentiation* 71:18–27.
20. Singh SK, et al. (2004) Identification of human brain tumour initiating cells. *Nature* 432:396–401.
21. Kim CF, et al. (2005) Identification of bronchioalveolar stem cells in normal lung and lung cancer. *Cell* 121:823–835.
22. O'Brien CA, Pollett A, Gallinger S, Dick JE (2007) A human colon cancer cell capable of initiating tumour growth in immunodeficient mice. *Nature* 445:106–110.
23. Hahn WC, Weinberg RA (2002) Rules for making human tumor cells. *N Engl J Med* 347:1593–1603.
24. Sherr CJ, McCormick F (2002) The RB and p53 pathways in cancer. *Cancer Cell* 2:103–112.

Strong interaction between the effects of alcohol consumption and smoking on oesophageal squamous cell carcinoma among individuals with *ADH1B* and/or *ALDH2* risk alleles

Fumiaki Tanaka,[1] Ken Yamamoto,[2] Sadao Suzuki,[3] Hiroshi Inoue,[1] Masahiko Tsurumaru,[4] Yoshiaki Kajiyama,[4] Hoichi Kato,[5] Hiroyasu Igaki,[5] Koh Furuta,[6] Hiromasa Fujita,[7] Toshiaki Tanaka,[7] Yoichi Tanaka,[8] Yoshiyuki Kawashima,[8] Shoji Natsugoe,[9] Tetsuro Setoyama,[9] Shinkan Tokudome,[3] Koshi Mimori,[1] Naotsugu Haraguchi,[1,10] Hideshi Ishii,[1,10] Masaki Mori[1,10]

► Additional figures and tables are published online only. To view these files please visit the journal online (http://gut.bmj.com).

[1]Department of Surgery, Medical Institute of Bioregulation, Kyushu University, Beppu, Japan
[2]Department of Molecular Genetics, Medical Institute of Bioregulation, Kyushu University, Fukuoka, Japan
[3]Department of Public Health, Nagoya City University Graduate School of Medical Sciences, Nagoya, Japan
[4]Department of Esophageal and Gastroenterological Surgery, Juntendo University School of Medicine, Tokyo, Japan
[5]Department of Surgery, National Cancer Center Hospital, Tokyo, Japan
[6]Division of Clinical Laboratories, National Cancer Center Hospital, Tokyo, Japan
[7]Department of Surgery, Kurume University School of Medicine, Kurume, Japan
[8]Division of Gastroenterological Surgery, Saitama Cancer Center, Saitama, Japan
[9]Department of Surgical Oncology and Digestive Surgery, Kagoshima University School of Medicine, Kagoshima, Japan
[10]Department of Gastroenterological Surgery, Osaka University Graduate School of Medicine, Osaka, Japan

Correspondence to
Dr Masaki Mori, Department of Gastroenterological Surgery, Osaka University Graduate School of Medicine, 2-2 Yamadaoka, Suita, Osaka, Japan 565-0871; mmori@gesurg.med.osaka-u.ac.jp

Revised 5 July 2010
Accepted 8 July 2010
Published Online First 9 September 2010

ABSTRACT

Background Oesophageal squamous cell carcinoma (OSCC) is considered a difficult cancer to cure. The detection of environmental and genetic factors is important for prevention on an individual basis.

Objective To identify groups at high risk for OSCC by simultaneously analysing both genetic and environmental risk factors.

Methods A multistage genome-wide association study of OSCC in Japanese individuals with a total of 1071 cases and 2762 controls was performed.

Results Two associated single-nucleotide polymorphisms (SNPs), as well as smoking and alcohol consumption, were evaluated as genetic and environmental risk factors, respectively, and their interactions were also evaluated. Risk alleles of rs1229984 (*ADH1B*) and rs671 (*ALDH2*) were highly associated with OSCC (odds ratio (OR)=4.08, $p=4.4\times10^{-40}$ and OR=4.13, $p=8.4\times10^{-76}$, respectively). Also, smoking and alcohol consumption were identified as risk factors for OSCC development. By integrating both genetic and environmental risk factors, it was shown that the combination of rs1229984 and rs671 risk alleles with smoking and alcohol consumption was associated with OSCC. Compared with subjects with no more than one environmental or genetic risk factor, the OR reached 146.4 (95% CI 50.5 to 424.5) when both environmental and genetic risk factors were present. Without the genetic risks, alcohol consumption did not correlate with OSCC. In people with one or two genetic risk factors, the combination of alcohol consumption and smoking increased OSCC risk.

Conclusions Analysis of *ADH1B* and *ALDH2* variants is valuable for secondary prevention of OSCC in high-risk patients who smoke and drink alcohol. In this study, SNP genotyping demonstrated that the *ADH1B* and/or *ALDH2* risk alleles had an interaction with smoking and, especially, alcohol consumption. These findings, if replicated in other groups, could demonstrate new pathophysiological pathways for the development of OSCC.

What is already known about this subject?

► Oesophageal squamous cell carcinoma (OSCC) is associated with drinking and smoking alcohol, but the genetic risk is unknown.

What are the new findings?

► This study demonstrates that single nucleotide polymorphisms of *ADH1B* and *ALDH2* interact with alcohol consumption, especially when combined with smoking, to increase OSCC risk.

How might they impact on clinical practice in the foreseeable future?

► The analysis of *ADH1B* and *ALDH2* variants would be valuable for individualised prevention of OSCC.

INTRODUCTION

Oesophageal squamous cell carcinoma (OSCC), but not adenocarcinoma, is relatively common in East Asia, including Japan.[1] Oesophageal cancer is the eighth most common cancer world wide, accounting for 462 000 new cases in 2002, and the sixth most common cause of cancer-related death (386 000 deaths). OSCC is the most common histological type world wide,[2] and is a treatment-resistant cancer that can withstand a combination of surgery, chemotherapy and radiotherapy.[1] It is difficult to diagnose OSCC early because it shows few symptoms in its early stages. Furthermore, there is no effective marker for predicting the development of OSCC. Therefore, it is important to detect risk factors for primary prevention and also to identify high-risk groups for secondary prevention.

Both genetic and environmental factors are involved in the pathogenesis of OSCC. Although smoking and alcohol consumption have been demonstrated as lifestyle factors that contribute to the development of the disease,[3] the DNA sequence variations that confer an additional risk of developing the disease remain largely unknown. The availability of high-resolution linkage disequilibrium (LD) maps and comprehensive sets of common single nucleotide polymorphisms (SNPs) that capture most of the common sequence

variations facilitate the identification of disease-related genes with genome-wide association studies, an approach without an a priori hypothesis based on a gene function or disease pathway.

To identify OSCC-related genes, we conducted a multistage genome-wide association study in Japanese individuals, with a total of 1071 cases and 2762 controls, and identified a significant genome-wide level of association for two and six SNPs on chromosomes 4q23 and 12q24.11-13, respectively. The most functional variants in the two regions, rs1229984 (*ADH1B*) and rs671 (*ALDH2*),[4] were strongly associated with OSCC. Furthermore, we analysed the association with OSCC of smoking and drinking alcohol, two of the principal environmental determinants of OSCC, both individually and jointly.[5] Finally, we evaluated the combined effects of environmental and genetic risk factors.

METHODS

Study sample

This case–control study was designed to investigate the environmental and genetic risk factors for OSCC. The eligibility criterion was that the oesophageal disease was pathologically diagnosed as OSCC. Patients with newly diagnosed oesophageal cancer, 35–85 years of age, were identified from six hospitals (Juntendo University Hospital, National Cancer Center Hospital, Kurume University Hospital, Saitama Cancer Center, Kagoshima University Hospital and Kyushu University Hospital) from 2000 to 2008. Healthy controls without a previous cancer history were recruited from Kyushu University Hospital (and related hospitals) during the same time period. All controls were enrolled after receiving an upper gastrointestinal endoscopy test to ensure that they had no disease. All participants provided written informed content. The study protocol was reviewed and approved by Kyushu University (Fukuoka, Japan), Juntendo University (Tokyo, Japan), National Cancer Center Hospital (Tokyo, Japan), Kurume University (Kurume, Japan), Saitama Cancer Center (Saitama, Japan) and Kagoshima University (Kagoshima, Japan). In total, 1071 patients with OSCC and 2762 controls were enrolled.

Environmental risk factors

Detailed information about demographic characteristics, lifestyle and daily diet was collected using a standardised questionnaire. Of all the known determinants of OSCC, we chose the two major ones—smoking and alcohol consumption—as environmental risk factors to investigate in detail. Information on smoking and alcohol consumption habits (eg, current smoker, ex-smoker, or non-smoker for smoking status) was collected at the time of enrolment. In addition, the Brinkman index (product of the number of cigarettes per day and years of smoking) for current smokers and years after quitting smoking or drinking (<1 year, 1–2 years, 3–9 years, or 10 years or longer) were calculated. Of the data collected from 1071 patients with OSCC and 2762 controls, the data from 742 patients with OSCC and 820 controls were analysed.

Genotyping, quality control and genetic association analysis

The genome-wide association study was carried out using the Affymetrix GeneChip Human Mapping 500K array (online supplementary figure 1). We genotyped 226 OSCC cases and 1118 controls using the Bayesian Robust Linear Model with Mahalanobis (BRLMM) algorithm. Samples with a genotype call rate <0.94 for either *Nsp*I or *Sty*I GeneChip SNPs were removed from analysis (N=12). To detect duplicated samples, relatives, and DNA-contaminated samples, pairwise identity-by-descent (IBD) estimation was carried out. We detected 1, 28 and 2 pairs showing IBD (PI_HAT) proportions of 1.0, approximately 0.5 and 0.25, respectively. Based on the results, 31 samples that had lower genotype call rates in each pair were excluded from the association analysis. In addition, we removed samples that had deviated averages of PI_HAT (approximately more than 3 standard deviations (PI_HAT > 0.020, N=13, see supplementary figure 2)) because such high mean PI_HAT values might be caused by DNA contamination or low-quality genotyping. These 13 samples also had higher rates of heterozygous genotypes than the other study samples (supplementary figure 3). After the sample quality check, 1288 samples (209 OSCC and 1079 controls) were subjected to further analysis.

SNPs were removed from analysis if they had a call rate of less than 0.95, showed a difference in call rate of more than 0.08 between OSCC and controls, displayed Hardy–Weinberg disequilibrium ($p<1.0\times10^{-4}$) in the control group, or had a minor allele frequency (MAF) <0.10. SNPs that were not selected in the updated GeneChip SNP5.0 (Affymetrix) were also excluded. After these exclusions, 234 830 SNPs remained in the first stage. The genomic inflation factor based on the median χ^2 value was 1.024 in this genome-wide association analysis (supplementary figure 4), implying that there was no systematic increase of false positives owing to population stratification or to any other form of bias. Six SNPs on chromosome 12q24 were strongly associated with the disease, exceeding the genome-wide significance level of $p=1.0\times10^{-7}$ (supplementary figure 5).

In the second stage, 480 OSCC and 864 control samples were genotyped using the Illumina Golden Gate Assay for the best 1536 SNPs (allelic p<0.013). When multiple SNPs displayed strong LD with each other ($r^2>0.8$), the most closely associated SNP was chosen to avoid redundancy during the selection of the 1536 SNPs. The samples with a genotype call rate <0.98 and SNPs with a call rate <0.98, Hardy-Weinberg disequilibrium ($p<1.0\times10^{-4}$) in the controls, or an MAF <0.05 were excluded from the association analysis. After quality control, 479 OSCC, 863 control and 1419 SNP samples remained, and 66 SNPs had an allele test p<0.05 at this stage.

Among the 26 SNPs that showed an allelic p<0.01 in the second stage, 25 could be genotyped with the TaqMan method in 365 OSCC cases and 780 controls in the third stage. The average SNP call rate of these 25 SNPs was 0.998. We identified 10 SNPs with an allelic p<0.05, and eight SNPs reached a significant genome-wide association level ($p<1\times10^{-7}$) in combined samples. The non-synonymous SNPs rs1229984 (*ADH1B*), rs671 (*ALDH2*) and rs16969968 (*CHRNA5*), as well as the synonymous SNP rs1051730 (*CHRNA3*), were also genotyped in all samples in the first through third stages by the TaqMan method.

Statistical analysis

To evaluate genetic and environmental factors, genotype data for the two SNPs (rs1229984 and rs671) and lifestyle data (smoking and alcohol consumption) were available for 742 OSCC cases and 820 controls. Odds ratios (OR) and 95% CIs (95% CIs) were calculated using unconditional logistic regression models, adjusted for sex, age (5-year categories) and study area (Honshu and Kyushu islands).

The environmental factors—that is, history of smoking and alcohol consumption, were re-categorised into two subclasses according to whether subjects had a previous habit of smoking or drinking; this was done to minimise the effect of disease. To evaluate the interaction effect more simply, we chose the

dominant or recessive model for both SNPs, combining the heterozygous group into either a wild homozygous or mutant homozygous group. The model was selected based on the fitness of the logistic regression. For the results, subjects with GA at rs1229984 were included in the group of AA homozygotes because the recessive model was a better fit than the dominant model. In contrast, the AG and AA genotypes of rs671 were combined because the dominant model was a better fit.

First, we estimated the environmental risk arising from smoking and alcohol consumption both individually and in combination (risk=0, 1 or 2). Similarly, for genetic risk, we estimated the OR of each factor of rs671 (AG/AA) and rs1229984 (GG) and their combined effect (risk=0, 1 or 2). Next, we repeated the same analysis for environmental risk according to the stratum of genetic risk. In the stratified analysis, we evaluated how the environmental effect was modified in the different genetic strata—that is, the existence of a gene—environment interaction. Here we used subjects with the AG/AA genotype of rs671 and/or GG genotype of rs1229984 as a genetic risk group. Finally, we calculated the risk number for the four risk factors in comparison with subjects who had no risk factors to evaluate the accumulation of risk (risk=0, 1, 2, 3 or 4) (tables 1, 2, and 3 and Figure 1).

p Values for the interaction are based on likelihood ratio tests that compared models with and without interaction terms.

Table 1 Characteristics of the cases and controls

Characteristics	Cases (N=742)		Controls (N=820)	
Sex				
Male	641	(86.4)	506	(61.7)
Female	101	(13.6)	314	(38.3)
Age (years)				
40–49	24	(3.2)	127	(15.5)
50–59	149	(20.1)	247	(30.1)
60–69	330	(44.5)	256	(31.2)
70–79	239	(32.2)	190	(23.2)
Environmental risk factor				
Non-drinker	63	(8.5)	341	(41.6)
Ever-drinker (environmental risk)	679	(91.5)	479	(58.4)
Non-smoker	103	(13.9)	422	(51.5)
Ever-smoker (environmental risk)	639	(86.1)	398	(48.5)
Environmental risk No=0	36	(4.9)	252	(30.7)
Environmental risk No=1	94	(12.7)	259	(31.6)
Environmental risk No=2	612	(82.5)	309	(37.7)
Genetic risk factor				
rs671 GG	194	(26.1)	502	(61.2)
rs671 AG/AA (genetic risk)	548	(73.9)	318	(38.8)
rs1229984 AA/AG	591	(79.6)	776	(94.6)
rs1229984 GG (genetic risk)	151	(20.4)	44	(5.4)
Genetic risk No=0	169	(22.8)	479	(58.4)
Genetic risk No=1	447	(60.2)	320	(39.0)
Genetic risk No=2	126	(17.0)	21	(2.6)
Total risk				
Total risk No=0	15	(2.0)	115	(14.0)
Total risk No=1	44	(5.9)	266	(32.4)
Total risk No=2	187	(25.2)	348	(42.4)
Total risk No=3	385	(51.9)	87	(10.6)
Total risk No=4	111	(15.0)	4	(0.5)

Results are shown as number (%).
No: The environmental risk arising from smoking and alcohol consumption, both individually and in combination (risk=0, 1 or 2). Similarly, for the genetic risk of each factor of rs671 (AG/AA) and rs1229984 (GG) and their combined effect (risk=0, 1 or 2). Finally, we calculated the risk number for the four risk factors in comparison with subjects who had no risk factors to evaluate the accumulation of risk (risk=0, 1, 2, 3 or 4).

Table 2 Risk of oesophageal squamous cell carcinoma associated with environmental and genetic risk factors and their internal interaction

Risk factors	Cases	Controls	OR	95% CI
Environmental risk factor				
Non-drinker and non-smoker (environmental risk No=0)	36	252	1.0	Reference
Ever-drinker and non-smoker (environmental risk No=1)	67	170	3.5	(2.1 to 5.8)
Non-drinker and ever-smoker (environmental risk No=1)	27	89	2.3	(1.2 to 4.3)
Ever-drinker and ever-smoker (environmental risk No=2)	612	309	16.0	(9.7 to 26.3)
p Value for interaction of drinking and smoking			0.048	
Genetic risk factor				
rs671 GG and rs1229984 AA/AG (genetic risk No=0)	169	479	1.0	Reference
rs671 AG/AA and rs1229984 AA/AG (genetic risk No=1)	422	297	4.8	(3.7 to 6.3)
rs671 GG and rs1229984 GG (genetic risk No=1)	25	23	3.1	(1.6 to 6.1)
rs671 AG/AA and rs1229984 GG (genetic risk No=2)	126	21	34.0	(18.1 to 63.8)
p Value for interaction of two genetic factors			0.079	

The odds ratios and the 95% CIs for oesophageal squamous cell carcinoma associated with alcohol consumption, smoking, and single nucleotide polymorphisms were estimated from logistic regression models adjusted for sex, age and study area. No: The environmental risk arising from smoking and alcohol consumption, both individually and in combination (risk=0, 1 or 2). Similarly, for the genetic risk of each factor—rs671 (AG/AA) and rs1229984 (GG)—and their combined effect (risk=0, 1 or 2). Finally, we calculated the risk number for the four risk factors in comparison with subjects who had no risk factors to evaluate the accumulation of risk (risk=0, 1, 2, 3 or 4).

Statistical analyses were performed with SAS software version 9.1 (SAS Institute). A two-tailed p value of <0.05 was considered statistically significant.

Genotype data cleaning and IBD analysis were carried out using PLINK version 1.06 software.[6] LD was assessed with HaploView version 4.0.[7] The statistical power for the allelic association analysis in the first and second stages of this study was calculated using the PS program[8] (supplementary table 1). Statistical analyses for the gene–environment interaction were performed with SAS. A two-tailed p value of <0.05 was considered statistically significant.

RESULTS

Figure 2 shows the study design. Table 1 shows several characteristics of the cases and controls. Cases included more men, older individuals, ever-drinkers, ever-smokers and subjects with the AG/AA genotype of rs671 and GG genotype of rs1229984 than controls. The average risk was significantly higher among cases (2.7) than among controls (1.5).

Our multistage association study identified two and six SNPs on chromosomes 4q23 and 12q24.11-13, respectively, which showed genome-wide evidence for association with OSCC ($p<1.0\times10^{-7}$) (table 4). The disease-associated markers of 4q23 spanned the *ADH* gene cluster region, including seven *ADH* family genes: *ADH1A, ADH1B, ADH1C, ADH4, ADH5, ADH6* and *ADH7* (Figure 3). We searched for functional SNPs in these genes in the SNP database and found one validated non-synonymous SNP in exon 3 of *ADH1B*, rs1229984, with an MAF >0.1 in the East Asian population. In addition, 12q24.12 contains the *ALDH2* gene, which is a well-known key enzyme in alcohol metabolism (Figure 4). This gene also possesses a non-synonymous SNP in exon 12, rs671, that affects its enzymatic activity. We assessed the LD between these functional SNPs and

Table 3 The risk of oesophageal squamous cell carcinoma associated with alcohol consumption and smoking status

Risk factors	rs671 GG and rs1229984 AA/AG (genetic risk No=0)		rs671 AG/AA or rs1229984 GG (genetic risk No=1 or 2)		p Value for interaction*
	OR	95% CI	OR	95% CI	
Environmental risk factor					
Non-drinker and non-smoker (environmental risk No=0)	1.0	Reference	1.1	(0.5 to 2.4)	
Ever-drinker and non-smoker (environmental risk No=1)	1.5	(0.7 to 3.3)	12.1	(5.5 to 26.6)	<0.001
Non-drinker and ever-smoker (environmental risk No=1)	4.5	(1.3 to 15.9)	2.4	(1.1 to 5.3)	0.44
Ever-drinker and ever-smoker (environmental risk No=2)	5.0	(2.5 to 10.1)	62.1	(30.3 to 127.4)	<0.001
p Value for interaction of drinking and smoking	0.55		0.048		

The odds ratios and 95% confidence intervals for oesophageal squamous call carcinoma associated with alcohol consumption and smoking were estimated from logistic regression models adjusted for sex, age, mutual habit and study area.
*p Value for interaction between genetic risk and drinking and/or smoking status.

associated SNP markers. We detected moderate LD between rs1229984 and rs1042026 as well as between rs671 and rs11066280 (r^2=0.66 and 0.87, respectively) in control samples (supplementary figure 5). These observations led us to examine the association of rs1229984 and rs671 with OSCC. We found a stronger association between these SNPs and OSCC (allele test OR=1.82, p $=6.2\times10^{-28}$ and OR =1.78, p $=1.0\times10^{-26}$ for rs1229984 and rs671, respectively) than between marker SNPs and OSCC (allele test OR=1.66, p$=1.8\times10^{-16}$ and OR=1.68, p$=2.5\times10^{-21}$ for rs1042026 on 4q23 and rs11066280 on 12q24, respectively), suggesting that rs1229984 and rs671 might be susceptibility variants for OSCC (table 4). Because the other SNP markers with disease associations reside in introns (eg, rs3805322 and rs2074356 reside in the introns of *ADH4* and *C12orf51*, respectively), we cannot exclude the possibility that they have a biological effect on genes from this region. However, other lines of evidence support a possible role for *ADH1B* and *ALDH2* in the pathogenesis of OSCC.

The risk alleles of rs1229984 in *ADH1B* (G) and rs671 in *ALDH2* (A) encode arginine-48 and lysine-504, respectively,

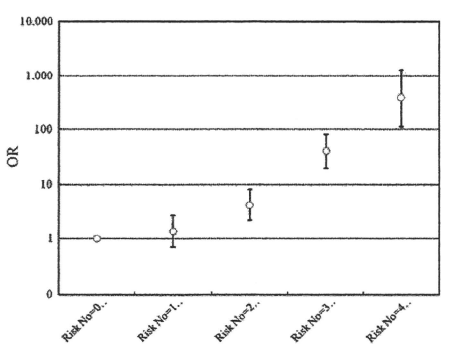

Figure 1 Magnitude of the risk of oesophageal squamous cell carcinoma (OSCC) associated with the number of environmental and genetic risk factors. The odds ratios (ORs) and the 95% CIs for OSCC associated with alcohol consumption, smoking and single nucleotide polymorphisms (rs671 GG and rs1229984) are estimated from logistic regression models adjusted for sex, age and study area. The data are shown as OR+95% CI. No: The environmental risk arising from smoking and alcohol consumption, both individually and in combination (risk=0, 1 or 2). Similarly, for the genetic risk of each factor—rs671 (AG/AA) and rs1229984 (GG)—and their combined effect (risk=0, 1 or 2). Finally, we calculated the risk number for the four risk factors in comparison with subjects who had no risk factors to evaluate the accumulation of risk (risk=0, 1, 2, 3 or 4).

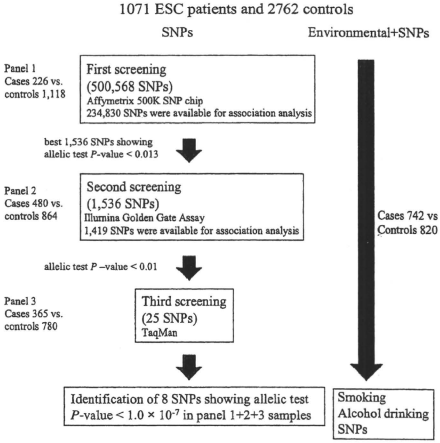

Figure 2 Design of the genome-wide association study and gene-environmental interaction study. In the first stage, 226 patients with oesophageal squamous cell carcinoma (ESC) and 1118 controls were genotyped for 500 568 single nucleotide polymorphisms (SNPs) by Affymetrix 500 K chip sets. Two additional rounds of screening by the Illumina Golden Gate Assay (1536 SNPs for the second screening) and TaqMan Assay (25 SNPs for the third screening) were performed as indicated. To evaluate genetic and environmental factors, genotype data for the two SNPs (rs1229984 and rs671) and lifestyle data (smoking and alcohol consumption) were available for 742 patients with ESC and 820 controls.